Inorg. Chem. **2002**, *41*, 86–107

Syntheses, Crystal Structures, and Density Functional Theory Calculations of the *closo*-[1-M(CO)$_3$(η^4-E$_9$)]$^{4-}$ (E = Sn, Pb; M = Mo, W) Cluster Anions and Solution NMR Spectroscopic Characterization of [1-M(CO)$_3$(η^4-Sn$_9$)]$^{4-}$ (M = Cr, Mo, W)†

Janette Campbell,‡ Hélène P. A. Mercier,*,‡ Holger Franke,‡ David P. Santry,§ David A. Dixon,|| and Gary J. Schrobilgen*,‡

Department of Chemistry, McMaster University, Hamilton, Ontario L8S 4M1, Canada, Snowbird Software, Inc., 71A Leland Street, Hamilton, Ontario, L8S 3A1, Canada, and William R. Wiley Environmental Molecular Sciences Laboratory, Pacific Northwest National Laboratory, 906 Battelle Boulevard, P.O. Box 999, KI-83, Richland, Washington 99352

Received July 2, 2001

The *closo*-[1-M(CO)$_3$(η^4-E$_9$)]$^{4-}$ (E = Sn, Pb; M = Mo, W) anions have been obtained by extracting the binary alloys KSn$_{2.05}$ and KPb$_{2.26}$ in ethylenediamine (en) in the presence of 2,2,2-crypt or in liquid NH$_3$ followed by reaction with M(CO)$_3$·mes (M = Mo, W) or Cr(CO)$_3$·tol in en or liquid NH$_3$ solution. Crystallization of the molybdenum and tungsten salts was induced by vapor diffusion of tetrahydrofuran into the en solutions. The salts [2,2,2-crypt-K]$_4$[1-M(CO)$_3$(η^4-Sn$_9$)]·en (M = Mo, W) crystallize in the triclinic system, space group $P\bar{1}$, $Z = 4$, $a = 16.187(3)$ Å, $b = 25.832(4)$ Å, $c = 29.855(5)$ Å, $\alpha = 111.46(1)°$, $\beta = 102.84(2)°$, $\gamma = 92.87(2)°$ at –95 °C (M = Mo) and $a = 17.018(3)$ Å, $b = 27.057(5)$ Å, $c = 28.298(6)$ Å, $\alpha = 66.42(3)°$, $\beta = 76.72(3)°$, $\gamma = 87.27(3)°$ at 20 °C (M = W). The salts (CO)$_3$M(en)$_2$[2,2,2-crypt-K]$_4$[1-M(CO)$_3$(η^4-Pb$_9$)]·2.5en (M = Mo, W) crystallize in the triclinic system, space group $P\bar{1}$, $Z = 2$, $a = 16.319(3)$ Å, $b = 17.078(3)$ Å, $c = 24.827(5)$ Å, $\alpha = 71.82(3)°$, $\beta = 83.01(3)°$, $\gamma = 81.73(3)°$ at –133 °C (M = Mo) and $a = 16.283(4)$ Å, $b = 17.094(3)$ Å, $c = 24.872(6)$ Å, $\alpha = 71.62(2)°$, $\beta = 82.91(2)°$, $\gamma = 81.35(2)°$ at –153 °C (M = W). The [1-M(CO)$_3$(η^4-Sn$_9$)]$^{4-}$ anions were also characterized in liquid NH$_3$ solution by ^{119}Sn, ^{117}Sn, and ^{95}Mo NMR spectroscopy. Unlike their fluxional precursor, *nido*-Sn$_9^{4-}$, NMR studies show that the [1-M(CO)$_3$(η^4-Sn$_9$)]$^{4-}$ anions are rigid on the NMR time scale. All possible inter- and intraenvironmental couplings, J(^{119,117}Sn–^{119,117}Sn), J(^{119,117}Sn–^{183}W), and one J(^{119,117}Sn–^{95}Mo) coupling, have been observed and assigned. Complete spin–spin coupling constant assignments were achieved by detailed analyses and simulations of all spin multiplets that comprise the ^{119}Sn and ^{117}Sn NMR spectra and that arise from natural abundance tin isotopomer distributions and from natural abundance ^{183}W, in the case of [1-W(CO)$_3$(η^4-Sn$_9$)]$^{4-}$. Both the solid state and solution structures of the [1-M(CO)$_3$(η^4-Sn$_9$)]$^{4-}$ anions are based on a closo-bicapped square antiprismatic structure in which the transition metal occupies a cap position. The cluster structures are consistent with Wade's rules for 22 ($2n + 2$) skeletal electron systems. Electron structure calculations at the density functional theory (DFT) level provide fully optimized geometries that are in agreement with the experimental structures. Complete assignment of the NMR spectra was also aided by GIAO calculations. The calculated vibrational frequencies of the E$_9^{4-}$ and [1-M(CO)$_3$-(η^4-E$_9$)]$^{4-}$ anions are also reported and are used to assign the solid-state vibrational spectra of the [1-M(CO)$_3$(η^4-E$_9$)]$^{4-}$ anions.

Introduction

Rudolph and co-workers,[1−4] who first identified naked cluster anions of the group 13−15 elements by solution ^{119}Sn, ^{205}Tl, and ^{207}Pb NMR spectroscopy, studied the homonuclear E$_9^{4-}$ (E = Sn, Pb) and the mixed series of isoelectronic anions Sn$_{9-x}$Ge$_x^{4-}$, Sn$_{9-x}$Pb$_x^{4-}$, and Sn$_{8-y}$Pb$_y$Tl^{5-} ($x = 0-9$, $y = 0-4$). The E$_9^{4-}$ anions (E = Si, Ge, Sn, Pb) and their

† Dedicated to Professor M. F. Hawthorne in appreciation for his contributions to the quality of American Chemical Society journals during his term as Editor of *Inorganic Chemistry* (1969−2000); presented at the 84th Canadian Society for Chemistry Conference, Montréal, Québec, May 26−30, 2001, Abstract No. 904-IN3.

* To whom correspondence should be sent. E-mail: SCHROBIL@MCMASTER.CA.

‡ McMaster University.

§ Snowbird Software, Inc.

|| Pacific Northwest National Laboratory.

(1) Rudolph, R. W.; Wilson, W. L.; Parker, F.; Taylor, R. C.; Young, D. C. *J. Am. Chem. Soc.* **1978**, *100*, 4629.

(2) Rudolph, R. W.; Taylor, R. C.; Young, D. C. In *Fundamental Research in Homogeneous Catalysis*; Tsutsui, M., Ed.; Plenum: New York, 1979; pp 997−1005.

(3) Rudolph, R. W.; Wilson, W. L.; Taylor, R. C. *J. Am. Chem. Soc.* **1981**, *103*, 2480.

(4) Wilson, W. L.; Rudolph, R. W.; Lohr, L. L.; Taylor, R. C.; Pyykko, P. *Inorg. Chem.* **1986**, *25*, 1535.

10.1021/ic010695k CCC: $22.00
Published on Web 12/13/2001

mixed analogues possess ($2n + 4$) skeletal electrons and are electron deficient. The structures are predicted to be, by the polyhedral skeletal electron pair theory (PSEPT) or Wade's rules,[5−7] nido-clusters derived from the parent ten-vertex deltahedron, a bicapped square antiprism. The X-ray crystal structures of the Si_9^{4-},[8] Ge_9^{4-},[9,10] Sn_9^{4-},[11,12] and Pb_9^{4-} [13,14] anions have been obtained and shown to possess nido-structures of $\sim C_{4v}$ symmetry, in accord with the PSEPT predictions.

The fluxionality of these nine-atom clusters has prevented their detailed structural characterization in solution by NMR spectroscopy. The observation of single ^{119}Sn, ^{207}Pb, and ^{205}Tl resonances and single $J(^{119}\text{Sn}-^{117}\text{Sn})$, $J(^{207}\text{Pb}-^{117,119}\text{Sn})$, $J(^{203,205}\text{Tl}-^{117,119}\text{Sn})$, and $J(^{203,205}\text{Tl}-^{207}\text{Pb})$ spin−spin couplings indicates that the three chemical environments of the C_{4v} structure are exchange-averaged by means of a facile intramolecular rearrangement process.[1−4] In the case of Sn_9^{4-} [1−4] and Pb_9^{4-},[1,2,4,13] intramolecular exchange averages the unique apical E(1), four coplanar E(2,3,4,5) atoms proximate to the apical atom, and the four coplanar E(6,7,8,9) atoms comprising the open nido-face of the cluster to a single chemical environment on the NMR time scale. Rapid rearrangement of the Pb_9^{4-} cluster prevents the observation of $J(^{207}\text{Pb}-^{207}\text{Pb})$ spin−spin couplings, because of chemical and magnetic equivalence. This contrasts with Sn_9^{4-}, which possesses two natural abundance magnetically active isotopes, ^{119}Sn and ^{117}Sn. A single exchange-averaged $J(^{119}\text{Sn}-^{117}\text{Sn})$ coupling constant is observed for Sn_9^{4-}, which results in an overlapping series of satellites corresponding to the summation of the binomial multiplet subspectra arising from the isotopomers $^{119}\text{Sn}_x{}^{117}\text{Sn}_y{}^{0}\text{Sn}_{9-(x+y)}{}^{4-}$ ($x + y = 0-9$), where ^{0}Sn denotes tin isotopes having zero spin. The fluxional behavior of the E_9^{4-} cluster anions is attributed to rapid intramolecular interconversion between nido-monocapped square antiprismatic (C_{4v}) and closo-tricapped trigonal prismatic (D_{3h}) structures by means of a C_{2v} transition state.[13,15,16] The mechanism is presumed to be operative for the related heteroanions. The barrier to $C_{4v}-D_{3h}$ interconversion in nine-atom clusters has been calculated using a points-on-a-sphere model for the pseudo-isoelectronic $B_9H_9^{2-}$ anion[15] and for Sn_9^{4-} by SCF-MO-CNDO calculations[16] and indicate a preference for D_{3h} symmetry in the gas phase. The barrier is less than 0.1% of the total orbital energy of either symmetry, suggesting that interconversion is likely to occur in solution. Local density functional theory (LDFT) calculations for Pb_9^{4-} show that the C_{4v} structure is favored in the gas phase. The low barrier to $C_{4v}-D_{3h}$ interconversion is also consistent with the low vibrational frequencies of the Pb_9^{3-} and Pb_9^{4-} anions,[13] intimating that the clusters are very deformable, and with the observation that fluxional behavior in Sn_9^{4-} and $TlSn_8^{5-}$ is not slowed in liquid NH_3 at temperatures as low as −74 °C.[3]

Rudolph and co-workers[17,18] were also the first to report the preparation of transition metal derivatives of the main-group metal clusters obtained by the reaction of $M'(PPh_3)_4$ with Sn_9^{4-} and Sn_8Tl^{5-} (M′ = Pt, Pd) and Pb_9^{4-} (M′ = Pt) in en (ethylenediamine). The resulting $Sn_9M'(PPh_3)_2^{4-}$, $Sn_8TlM'(PPh_3)_2^{5-}$, and $Pb_9PtL_2^{4-}$ (L = PPh_3 and/or en) anions were shown to be fluxional in solution by ^{31}P, ^{119}Sn, ^{205}Tl, and ^{207}Pb NMR spectroscopy; however, no ^{195}Pt resonances were reported. Rudolph and co-workers[17,18] were unable to establish whether the clusters were nido- or closo-structures by use of multi-NMR spectroscopy.

To date, the only closo-transition metal derivatives of electron-deficient naked metal main-group clusters that have been reported and structurally characterized by X-ray crystallography are the [1-Cr(CO)$_3$(η^4-E$_9$)]$^{4-}$ (E = Sn,[19,20] Pb[21]), [2-W(CO)$_3$(η^5-Sn$_9$)]$^{4-}$,[20] $Sn_6[M(CO)_5]_6^{2-}$,[22] and $Ge_6[M(CO)_5]_6^{2-}$ [22] (M = Cr, Mo, W) cluster anions. In accord with the ($2n$ +2) rule for closo-clusters having 22 and 14 skeletal electrons, both the endo-skeletal Cr(CO)$_3$, W(CO)$_3$ and exo-skeletal M(CO)$_5$ groups donate zero electrons to the skeletal bonding of these anions. The [1-Cr(CO)$_3$(η^4-E$_9$)]$^{4-}$ and [2-W(CO)$_3$(η^5-Sn$_9$)]$^{4-}$ anions are representative of the reaction products expected between nido-clusters and a zero-electron donor. Two related closo-metalloborane isomers derived from $B_9H_{12}^-$ and having 22 skeletal electrons have also been reported, i.e., *closo*-[(η^5-C$_5$H$_5$)-1-Ni(η^4-B$_9$H$_9$)]$^-$ [23,24] and *closo*-[(η^5-C$_5$H$_5$)-2-Ni(η^5-B$_9$H$_9$)]$^-$.[23,24]

In view of the facile intramolecular exchange behavior exhibited by the 22-electron *nido*-Sn_9^{4-} and *nido*-Pb_9^{4-} anions and by related isovalent anions, it was of interest to determine what type, if any, intramolecular exchange processes might arise when the zero-electron donor transition metal fragments M(CO)$_3$ (M = Cr, Mo, W) are coordinated to the nido-faces of E_9^{4-} anions.

At the point of submission of this paper, we learned of an independent study on the $[M(CO)_3Sn_9]^{4-}$ (M = Cr, Mo, W) anions by Eichhorn et al., who have obtained similar spectra,

(5) Wade, K. *Adv. Inorg. Radiochem.* **1976**, *18*, 1.
(6) Mingos, D. M. P. *Acc. Chem. Res.* **1984**, *17*, 311.
(7) Mingos, D. M. P. *J. Chem. Soc., Chem. Commun.* **1983**, 706.
(8) von Schnering, H. G.; Somer, M.; Kaupp, M.; Carrillo-Cabrera, W.; Baitinger, M.; Schmeding, A.; Grin, Y. *Angew. Chem., Int. Ed. Engl.* **1998**, *37*, 2359.
(9) Diehl, L.; Khodadadeh, K.; Kummer, D.; Strähle, J. *Chem. Ber.* **1976**, *109*, 3404.
(10) Belin, C. H. E.; Corbett, J. D.; Cisar, A. *J. Am. Chem. Soc.* **1977**, *99*, 7163.
(11) Corbett, J. D.; Edwards, P. A. *J. Am. Chem. Soc.* **1977**, *99*, 3313.
(12) Burns, R. C.; Corbett, J. D. *Inorg. Chem.* **1985**, *24*, 1489.
(13) Campbell, J.; Dixon, D. A.; Mercier, H. P. A.; Schrobilgen, G. J. *Inorg. Chem.* **1995**, *34*, 5798.
(14) Korber, N.; Fleischmann, A. *J. Chem. Soc., Dalton Trans.* **2001**, 383.
(15) Guggenberger, L. J.; Muetterties E. L. *J. Am. Chem. Soc.* **1976**, *98*, 7221.
(16) Burns, R. C.; Gillespie, R. J.; Barnes, J. A.; McGlinchey, M. J. *Inorg. Chem.* **1982**, *21*, 799.
(17) Teixidor, F.; Luetkens, M. L., Jr.; Rudolph, R. W. *J. Am. Chem. Soc.* **1983**, *105*, 149.
(18) Luetkens, M. L., Jr.; Teixidor, F.; Rudolph, R. W. *Inorg. Chim. Acta* **1984**, *83*, L13.
(19) Eichhorn, B. W.; Haushalter, R. C.; Pennington, W. T. *J. Am. Chem. Soc.* **1988**, *110*, 8704.
(20) Kesanli, B.; Fettinger, J.; Eichhorn, B. W. *Chem.−Eur. J.* **2001**, in press.
(21) Eichhorn, B. W.; Haushalter, R. C. *J. Am. Chem. Soc., Chem. Commun.* **1990**, 937.
(22) Renner, G.; Kircher, P.; Huttner, G.; Rutsch, P.; Heinze, K. *Eur. J. Inorg. Chem.* **2001**, 973.
(23) Leyden, R. N.; Hawthorne, M. F. *J. Chem. Soc., Chem. Commun.* **1975**, 310.
(24) Leyden, R. N.; Sullivan, B. P.; Baker, R. T.; Hawthorne, M. F. *J. Am. Chem. Soc.* **1978**, *100*, 3758.

Table 1. Summary of Crystal Data and Refinement Results for [2,2,2-crypt-K]$_4$[1-M(CO)$_3$(η^4-Sn$_9$)]·en and M(CO)$_3$(en)$_2$[2,2,2-crypt-K]$_4$[1-M(CO)$_3$(η^4-Pb$_9$)]·2.5en (M = Mo, W)

	[2,2,2-crypt-K]$_4$[1-M(CO)$_3$(η^4-Sn$_9$)]·en		M(CO)$_3$(en)$_2$[2,2,2-crypt-K]$_4$[1-M(CO)$_3$(η^4-Pb$_9$)]·2.5en	
formula	$C_{77}H_{152}K_4MoN_{10}O_{27}Sn_9$	$C_{77}H_{152}K_4N_{10}O_{27}Sn_9W$	$C_{87}H_{180}K_4Mo_2N_{17}O_{30}Pb_9$	$C_{87}H_{180}K_4N_{17}O_{30}Pb_9W_2$
fw	2970.64	3046.54	4157.47	4333.29
space group (no.)	$P\bar{1}$ (2)	$P\bar{1}$ (2)	$P\bar{1}$ (2)	$P\bar{1}$ (2)
a (Å)	16.187(3)	17.018(3)	16.319(3)	16.283(4)
b (Å)	25.832(4)	27.057(5)	17.078(3)	17.094(3)
c (Å)	29.855(5)	28.298(6)	24.827(5)	24.872(6)
α (deg)	111.46(1)	66.42(3)	71.82(3)	71.62(2)
β (deg)	102.84(2)	76.72(3)	83.01(3)	82.91(2)
γ (deg)	92.87(2)	87.27(3)	81.73(3)	81.35(2)
V (Å^3)	11208.3(33)	11608.13(44)	6483.7(21)	6473.9(24)
Z	4	4	2	2
T (°C)	−95	20	−133	−153
λ (Å)	0.71073	0.71073	0.71073	0.71073
ρ_{calcd} (g cm^{-3})	1.760	1.743	2.130	2.223
μ (mm^{-1})	2.293	3.095	12.022	13.621
R_1[a]	0.0982	0.1215	0.0700	0.0544
wR_2[b]	0.2759	0.3794	0.1781	0.1227

[a] $R_1 = \sum||F_o| - |F_c||/\sum|F_o|$ for $I > 2\sigma(I)$. [b] $wR_2 = [\sum[w(F_o^2 - F_c^2)^2]/\sum w(F_o^2)^2]^{1/2}$ for $I > 2\sigma(I)$.

but of lower resolution, and have interpreted the spectra in terms of a dynamic equilibrium between the η^4- and η^5 isomers.[20]

The present paper[25] reports the crystal structures of the heteroatomic *closo*-[1-M(CO)$_3$(η^4-E$_9$)]$^{4-}$ anions (E = Sn, Pb; M = Mo, W) and the comprehensive solution characterizations of the *closo*-[1-M(CO)$_3$(η^4-Sn$_9$)]$^{4-}$ (M = Cr, Mo, W) anions by ^{119}Sn, ^{117}Sn, and ^{95}Mo NMR spectroscopy. A preliminary study of the *closo*-[1-Mo(CO)$_3$(η^4-Pb$_9$)]$^{4-}$ anion by ^{207}Pb NMR spectroscopy is also described. The solution NMR studies provide a means to study the effect on the cluster dynamics upon coordination of a zero-electron donor group to an otherwise fluxional *nido*-E$_9^{4-}$ cluster. In contrast with the study of Eichhorn et al., the present solution study definitively establishes that the *closo*-[1-M(CO)$_3$(η^4-Sn$_9$)]$^{4-}$ (M = Cr, Mo, W) anions are rigid on the NMR time scale. Density functional theory calculations have been done at the LDFT level to support and aid in the assignments of the experimental NMR and vibrational spectra and to provide a better understanding of the nature of the bonding between naked main-group metal clusters and transition metals.

Results and Discussion

X-ray Crystal Structures of the *closo*-[1-M(CO)$_3$(η^4-E$_9$)]$^{4-}$ Anions (E = Sn, Pb; M = Mo, Cr). Details of synthetic and crystal growing procedures are given in the Experimental Section and details of data collection parameters and other crystallographic information are given in Table 1. The most significant E−E and E−M contacts, E···E long contact distances, and M−C and C−O bond lengths in the [1-M(CO)$_3$(η^4-E$_9$)]$^{4-}$ anions are given in Table 2. Bond angles are included in the Supporting Information. The bicapped square antiprismatic geometries observed for the [1-M(CO)$_3$(η^4-E$_9$)]$^{4-}$ clusters are shown in Figure 1 along with the atom numbering scheme used throughout this paper. The structures of the (2,2,2-crypt-K$^+$·en) cations and the M(CO)$_3$(en)$_2$ complexes associated with the 1-M(CO)$_3$(η^4-Pb$_9^{4-}$) are illustrated in Figures S1 and S2 of the Supporting Information.

The most important features of these structures are the heteroatomic [1-M(CO)$_3$(η^4-E$_9$)]$^{4-}$ (M = Mo, W) anion clusters (Figure 1). All four anions exhibit the bicapped square antiprismatic geometries predicted by PSEPT for (2*n* + 2) skeletal electron systems and contain M(CO)$_3$ fragments which occupy the otherwise open square faces of the parent *nido*-E$_9^{4-}$ anions. The *closo*-[1-M(CO)$_3$(η^4-E$_9$)]$^{4-}$ anions are isostructural with the known [1-Cr(CO)$_3$(η^4-E$_9$)]$^{4-}$ analogues[19−21] as well as with the *closo*-[(η^5-C$_5$H$_5$)-1-Ni(η^4-B$_9$H$_9$)]$^-$ metalloborane[23,24] and the heteroatom-substituted XB$_9$H$_9$ (X = BH^{2-},[26] CH$^-$,[27] NH,[28] S[29]) clusters. The [1-M(CO)$_3$(η^4-Pb$_9$)]$^{4-}$ anions possess essentially C_s point group symmetry, whereas the [1-M(CO)$_3$(η^4-Sn$_9$)]$^{4-}$ anions possess C_1 point group symmetry. The symmetry differences arise from the orientation of the M(CO)$_3$ group relative to the E$_9$ cage.[30] The E−E contacts (Table 2) within the E$_9$-framework of [1-M(CO)$_3$(η^4-E$_9$)]$^{4-}$ can be classified into three categories: the shortest E−E contacts are those from the apical E(1) atoms to the E(2,3,4,5) planes and those within the E(6,7,8,9) planes; longer contacts are observed between the two E$_4$-planes of the square antiprisms; and the longest contacts exist between the adjacent E atoms of the E(2,3,4,5) planes. A comparison of the E−E contacts between the *nido*-E$_9^{4-}$ precursors and the *closo*-[1-M(CO)$_3$-(η^4-E$_9$)]$^{4-}$ anions reveals that coordination of the M(CO)$_3$ fragments to the E(6,7,8,9) planes results in elongation of the E−E distances within these planes. The E−E distances

(25) The X-ray crystal sructures, experimental NMR spectra with their full assignments, and infrared data were originally reported in the Ph.D. Thesis of J. Campbell (McMaster University, 1997).

(26) Hawthorne, M. F.; Pilling, R. L.; Stokely, P. F. *J. Am. Chem. Soc.* **1965**, *87*, 1893.

(27) Knoth, W. H. *Inorg. Chem.* **1971**, *10*, 598.

(28) Arafat, A.; Baer, J.; Huffman, J. C.; Todd, L. J. *Inorg. Chem.* **1986**, *25*, 3797.

(29) Pretzer, W. R.; Rudolph, R. W. *J. Am. Chem. Soc.* **1973**, *95*, 931.

(30) For structural conformers possessing C_s symmetry, one CO group eclipses an E atom of the E(2,3,4,5) plane while it is staggered with respect to the E(6,7,8,9) plane. All three CO groups of the C_1 conformers are gauche with respect to the E atoms of the E(2,3,4,5) and E(6,7,8,9) rings, so no CO groups lie in a mirror plane of the ME$_9$ bicapped square antiprism.

Table 2. The E−E, E−M, M−C, and C−O Distances (Å) in the [1-M(CO)$_3$(η^4-E$_9$)]$^{4-}$ (E = Sn, Pb; M = Mo, W) Anions

	Sn$_9$Mo(CO)$_3^{4-}$ [a]	Sn$_9$W(CO)$_3^{4-}$ [a]	Pb$_9$Mo(CO)$_3^{4-}$	Pb$_9$W(CO)$_3^{4-}$
		E−E Contacts from the Apical E(1) Atom to the E(2,3,4,5) Plane		
E(1)−E(2)	2.959(2), 2.967(3)	2.955(5), 2.954(4)	3.0661(10)	3.0330(11)
E(1)−E(3)	2.919(2), 2.950(2)	2.946(3), 2.966(3)	3.0533(10)	3.0557(10)
E(1)−E(4)	2.958(2), 2.961(3)	2.978(3), 2.977(3)	3.0326(14)	3.0737(9)
E(1)−E(5)	2.954(2), 2.947(2)	2.935(3), 2.937(3)	3.0407(9)	3.0417(9)
		E−E Contacts and E···E Long Contact Distances within the E(2,3,4,5) Plane		
E(2)−E(3)	3.187(3), 3.216(3)	3.209(4), 3.201(3)	3.3094(14)	3.3076(10)
E(2)−E(5)	3.170(2), 3.155(3)	3.167(4), 3.161(3)	3.3165(12)	3.3282(11)
E(3)−E(4)	3.283(2), 3.146(3)	3.192(3), 3.189(3)	3.3200(12)	3.3050(11)
E(4)−E(5)	3.137(2), 3.189(2)	3.225(3), 3.213(3)	3.3289(14)	3.3086(10)
E(2)···E(4)	4.527(3), 4.502(3)	4.550(4), 4.529(3)	4.696(2)	4.691(1)
E(3)···E(5)	4.507(2), 4.482(2)	4.495(3), 4.495(3)	4.690(2)	4.678(1)
		E−E Contacts between the E(2,3,4,5) and E(6,7,8,9) Planes		
E(2)−E(6)	2.976(2), 2.946(2)	2.984(3), 3.000(3)	3.1399(9)	3.1184(9)
E(2)−E(9)	2.978(2), 2.926(2)	2.979(3), 2.985(3)	3.1248(11)	3.1136(8)
E(3)−E(6)	2.950(2), 2.939(2)	2.968(4), 2.970(3)	3.1527(10)	3.0854(10)
E(3)−E(7)	2.961(2), 2.959(2)	2.977(3), 2.978(3)	3.0844(13)	3.1703(8)
E(4)−E(7)	2.946(2), 2.984(2)	2.990(3), 3.001(3)	3.1082(9)	3.1471(10)
E(4)−E(8)	2.939(2), 2.968(2)	2.963(3), 2.972(3)	3.1059(9)	3.1289(9)
E(5)−E(9)	2.998(2), 2.984(2)	2.981(4), 2.962(3)	3.1200(9)	3.0813(10)
E(5)−E(8)	2.995(2), 2.980(2)	2.969(3), 2.977(3)	3.0765(11)	3.1364(8)
		E−E Contacts and E···E Long Contact Distances within the E(6,7,8,9) Plane		
E(6)−E(9)	3.064(2), 3.082(2)	3.095(3), 3.094(3)	3.1489(11)	3.2962(10)
E(6)−E(7)	3.096(2), 3.102(2)	3.049(3), 3.035(3)	3.2026(12)	3.2171(10)
E(7)−E(8)	3.053(2), 3.082(2)	3.094(3), 3.099(3)	3.2911(11)	3.1466(9)
E(8)−E(9)	3.029(2), 3.073(2)	3.115(3), 3.080(3)	3.1842(12)	3.1948(10)
E(7)···E(9)	4.329(2), 4.356(2)	4.412(3), 4.374(3)	4.556(2)	4.517(1)
E(6)···E(8)	4.327(2), 4.368(2)	4.323(3), 4.329(3)	4.513(1)	4.571(1)
		E−M Contacts		
E(6)−M(10)	2.976(2), 2.993(2)	2.947(2), 2.955(2)	3.052(2)	3.0081(8)
E(7)−M(10)	2.984(2), 2.999(2)	3.029(2), 3.020(2)	3.0055(12)	3.0347(10)
E(8)−M(10)	3.004(2), 3.004(2)	2.997(2), 2.999(2)	2.9852(11)	3.0768(10)
E(9)−M(10)	3.028(2), 2.946(2)	2.952(2), 2.951(2)	3.0840(13)	2.9902(9)
		M−C Bond Lengths		
M(10)−C(11)	1.89(2), 1.77(2)	1.88(3), 1.98(3)	1.950(13)	1.939(9)
M(10)−C(12)	1.87(2), 1.86(3)	1.87(2), 1.94(2)	1.926(10)	1.928(13)
M(10)−C(13)	1.88(2), 1.84(2)	1.95(2), 1.87(2)	1.926(12)	1.935(12)
		C−O Bond Lengths		
C(11)−O(11)	1.16(2), 1.27(2)	1.22(3), 1.09(3)	1.19(2)	1.189(11)
C(12)−O(12)	1.21(2), 1.20(3)	1.26(3), 1.17(3)	1.175(13)	1.186(14)
C(13)−O(13)	1.21(2), 1.27(3)	1.12(3), 1.24(3)	1.189(14)	1.171(14)

[a] Values are for the two noncrystallographically equivalent anions defined in the asymmetric unit.

within the E(6,7,8,9) planes increase in the order Cr < Mo < W, with these increases being larger for the lead series than for the tin series. The distances within the E(2,3,4,5) plane show the opposite, less pronounced trend over the chromium triad, but are larger than those of the E(6,7,8,9) plane coordinated to the metal. The E−E contacts from the capping E(1) atoms to the adjacent E(2,3,4,5) plane and between the two square planes in the [1-M(CO)$_3$(η^4-E$_9$)]$^{4-}$ anions are similar to those in the E$_9^{4-}$ anions.

The Sn−Mo [2.977(2)−3.028(2) Å] and Sn−W [2.949(2)−3.030(2) Å] distances (Table 2) are significantly longer than the sums of their respective single-bond metallic radii [2.695 and 2.703 Å].[31] Similarly, the Pb−Mo [2.9852(11)−3.0839(13) Å] and Pb−W [2.9902(2)−3.0768(10) Å] distances are also longer than the sums of their respective single-bond metallic radii [2.834 and 2.842 Å, respectively].[31] The Sn−M distances in the [1-M(CO)$_3$(η^4-Sn$_9$)]$^{4-}$ (M = Mo, W) anions are longer than those in Sn$_6$[M(CO)$_5$]$_6^{2-}$,[22] Tl(O^{t}Bu)$_3$Sn−Mo(CO)$_5$,[32] (CO)$_5$Mo−Sn(O^{t}Bu)$_3$In−Mo(CO)$_5$,[32] [(μ_3-OH)(μ_3-O)$_3$(OEt)$_3$\{(CO)$_5$W\}$_7$Sn$_7$]$^{2-}$,[33] and (CO)$_5$WSn[W(CO)$_5$]$_2$.[34] The Pb−Mo distances in [1-Mo(CO)$_3$(η^4-Pb$_9$)]$^{4-}$ are comparable to the Pb−Mo bond length in (C$_5$H$_5$)(CO)$_3$MoPbPh$_3$,[35] but they are longer than the Pb−Mo bonds in [(C$_5$H$_5$)$_2$HMo]$_2$Pb(O$_2$CCH$_3$)$_2$.[36] The M−C and C−O bond lengths in the [1-M(CO)$_3$(η^4-E$_9$)]$^{4-}$ anions (Table 2) are in close agreement with other values reported in the literature[19−22,32−34] and are equal, within experimental error, to those of M(CO)$_3$(en)$_2$ reported in this study.

The structure of M(CO)$_3$(en)$_2$ and the coordination of en solvent molecules are discussed in the Supporting Information.

Characterization of the [1-M(CO)$_3$(η^4-Sn$_9$)]$^{4-}$ (M = Cr, Mo, W) Anions by NMR Spectroscopy. The [1-M(CO)$_3$-

(31) Pauling, L. In *Nature of the Chemical Bond*, 3rd ed.; Cornell University Press: Ithaca, NY, pp 116, 256, 261.
(32) Veith, M.; Kunze, K. *Angew. Chem., Int. Ed. Engl.* **1991**, *30*, 95.
(33) Kircher, P.; Huttner, G.; Zsolnai, L.; Driess, A. *Angew. Chem., Int. Ed. Engl.* **1998**, *37*, 1666.
(34) Huttner, G.; Weber, U.; Sigwarth, B.; Scheidsteger, O.; Lang, H.; Zsolnai, L. *J. Organomet. Chem.* **1985**, *282*, 331.
(35) Struchkov, Y. T.; Anisimov, K. N.; Osipova, O. P.; Kolobova, N. E.; Nesmeyanov, A. N. *Dokl. Akad. Nauk SSSR* **1967**, *172*, 107.
(36) Kubicki, M. M.; Kergoat, R,; Guerchais, J.-E. *J. Chem. Soc., Dalton Trans.* **1984**, 1791.

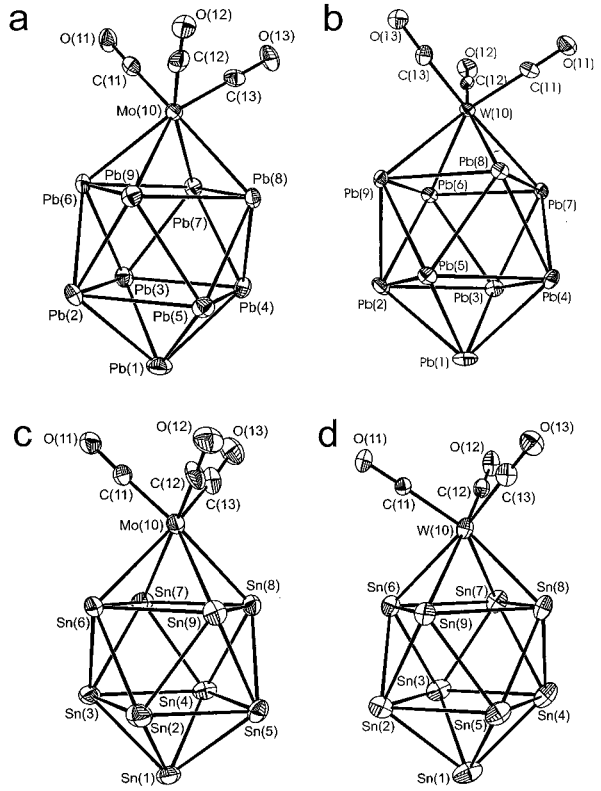

Figure 1. Structures of the (a) [1-Mo(CO)$_3$(η^4-Pb$_9$)]$^{4-}$, (b) [1-W(CO)$_3$-(η^4-Pb$_9$)]$^{4-}$, (c) [1-Mo(CO)$_3$(η^4-Sn$_9$)]$^{4-}$, and (d) [1-W(CO)$_3$(η^4-Sn$_9$)]$^{4-}$ anions. Thermal ellipsoids are shown at the 50% probability level.

(η^4-Sn$_9$)]$^{4-}$ anions were structurally characterized in liquid NH_3 solutions by observation of the spin-$^1/_2$ nuclides ^{119}Sn, ^{117}Sn, and ^{95}Mo at their natural abundance levels. All ^{119}Sn and ^{117}Sn NMR spectra were recorded at 0 °C, while the ^{119}Sn, ^{117}Sn, and ^{95}Mo spectra of [1-Mo(CO)$_3$(η^4-Sn$_9$)]$^{4-}$ were also recorded at 30 °C in order to minimize the effects of solvent viscosity on the rate of quadrupolar relaxation and line broadening.

The experimental ^{119}Sn, ^{117}Sn, and ^{95}Mo NMR spectra for the [1-M(CO)$_3$(η^4-Sn$_9$)]$^{4-}$ (M = Cr, Mo, W) anions at 0 °C in liquid NH_3 are depicted in Figures 2−6 and display three tin environments in a 4:4:1 intensity ratio along with accompanying ^{119}Sn, ^{117}Sn, and ^{183}W satellites.[37] The observation of three tin resonances indicates that the M(CO)$_3$ groups are unhindered and rotate sufficiently rapidly about the Sn(1)−M pseudo 4-fold axis of the MSn$_9$ cage, so the M(CO)$_3$ tripods do not lower the 4-fold symmetries of MSn$_9$ cages on the NMR time scale. The possibility that the Sn-(2,3,4,5) and Sn(6,7,8,9) rings are rotating relative to each other has been considered. This intramolecular exchange process is definitively shown in the subsequent discussion to be inconsistent with the observed number of interplanar coupling paths. The chemical shifts and spin−spin coupling constants extracted from the satellite spectra are summarized in Tables 3 and 4. The number of environments, the satellite spacings corresponding to J(^{119}Sn−^{119}Sn), J(^{119}Sn−^{117}Sn), J(^{117}Sn−^{117}Sn), J(^{117,119}Sn−^{95}Mo), and J(^{117,119}Sn−^{183}W), and the satellite-to-central peak intensity ratios are consistent with bicapped square antiprismatic MSn$_9$ structures having apparent C_{4v} point symmetries (unhindered M(CO)$_3$ rotation) on the NMR time scale and with the solid-state geometries of the [1-M(CO)$_3$(η^4-Sn$_9$)]$^{4-}$ anions.

The NMR study not only shows that the structures of these anions are retained in solution, but in contrast with the *nido*-Sn$_9^{4-}$ precursor, the 10-vertex *closo*-MSn$_9$ cages are stereochemically rigid on the NMR time scale. Assignments of the three tin resonances and the major ^{117}Sn, ^{119}Sn, and ^{183}W satellite spectra of the [1-M(CO)$_3$(η^4-Sn$_9$)]$^{4-}$ anions that led to the deduction of their solution structures are discussed below.

(a) Chemical Shifts. The most deshielded resonance is readily assigned to the apical Sn(1) based on its relative intensity. The assignments of the resonances corresponding to the two planes, Sn(2,3,4,5) and Sn(6,7,8,9), are based on their relative atomic charges (see below and Computational Results) and are confirmed by the relative magnitudes of the ^{119}Sn−^{117}Sn, ^{119}Sn−^{119}Sn, and ^{117}Sn−^{117}Sn couplings between these planes and the apical Sn(1) atom (see Spin−Spin Coupling in [1-M(CO)$_3$(η^4-Sn$_9$)]$^{4-}$). As a consequence, the most shielded of the three resonances is assigned to the Sn(2,3,4,5) plane adjacent to the apical Sn(1) atom and that having intermediate shielding is assigned to the Sn(6,7,8,9) plane for each anion of the series.

The ^{119}Sn NMR resonance of the apical Sn(1) atom in [1-M(CO)$_3$(η^4-Sn$_9$)]$^{4-}$ is very significantly deshielded [2493.2 (Cr), 2125.1 (Mo), and 2448.2 (W) ppm] relative to the Sn-(2,3,4,5) [−521.9 (Cr), −682.1 (Mo), and −735.7 (W) ppm] and Sn(6,7,8,9) environments [−213.9 (Cr), −402.4 (Mo), and −496.9 (W) ppm]. A pronounced deshielding of the apical atoms in bicapped antiprismatic clusters has also been observed in heteroatom-substituted boranes.[26−29,38−40] For example, in the ^{11}B NMR spectrum of the nonfluxional [(η^5-C$_5$H$_5$)-1-Ni(η^4-B$_9$H$_9$)]$^-$ cluster,[23,24] the resonance corresponding to the B(1) atom appears at 73.6 ppm, whereas those corresponding to the two B$_4$-planes appear at 29.0 and −1.3 ppm; however, the resonances could not be unambiguously assigned to the B(2,3,4,5) and B(6,7,8,9) planes. The shift to higher frequency for the apical B atom located opposite the apical heteroatom in a closo-cluster has been termed the "antipodal effect".[38−40]

Addition of the M(CO)$_3$ group to the Sn$_9^{4-}$ cluster results in appreciable changes in the ^{119}Sn chemical shifts of the [1-M(CO)$_3$(η^4-Sn$_9$)]$^{4-}$ anions relative to that of Sn$_9$.$^{4-}$ This behavior contrasts with the relative insensitivity of the ^{119}Sn chemical shifts for the Sn$_9$M′(PPh$_3$)$_2^{4-}$ and Sn$_8$TlM′(PPh$_3$)$_2^{5-}$ anions upon replacement of a Pt(PPh$_3$)$_2$ group with a Pd-(PPh$_3$)$_2$ group.[17,18] The weighted averages of the ^{119}Sn NMR resonances of the [1-M(CO)$_3$(η^4-Sn$_9$)]$^{4-}$ anions all occur to

(37) In addition to the three intense resonances of the [1-W(CO)$_3$(η^4-Sn$_9$)]$^{4-}$ anion and the *nido*-Sn$_9^{4-}$ anion (−1291.9 ppm, J(^{119}Sn−^{117}Sn) = 280 Hz)), two weak singlets were observed in the Sn$_9^{4-}$/W(CO)$_3$·mes system, but they could not be assigned due to their low intensity [δ-(^{119}Sn) = −639 ppm; δ(^{119}Sn) = −712 ppm].

(38) Heřmánek, S. *Chem. Rev.* **1992**, *92*, 325.
(39) Heřmánek, S.; Hnyk, D.; Havlas, Z. *J. Chem. Soc., Chem. Commun.* **1989**, 1859.
(40) Bühl, M.; Schleyer, P. v. R.; Havlas, Z.; Hnyk, D.; Heřmánek, S. *Inorg. Chem.* **1991**, *30*, 3107.

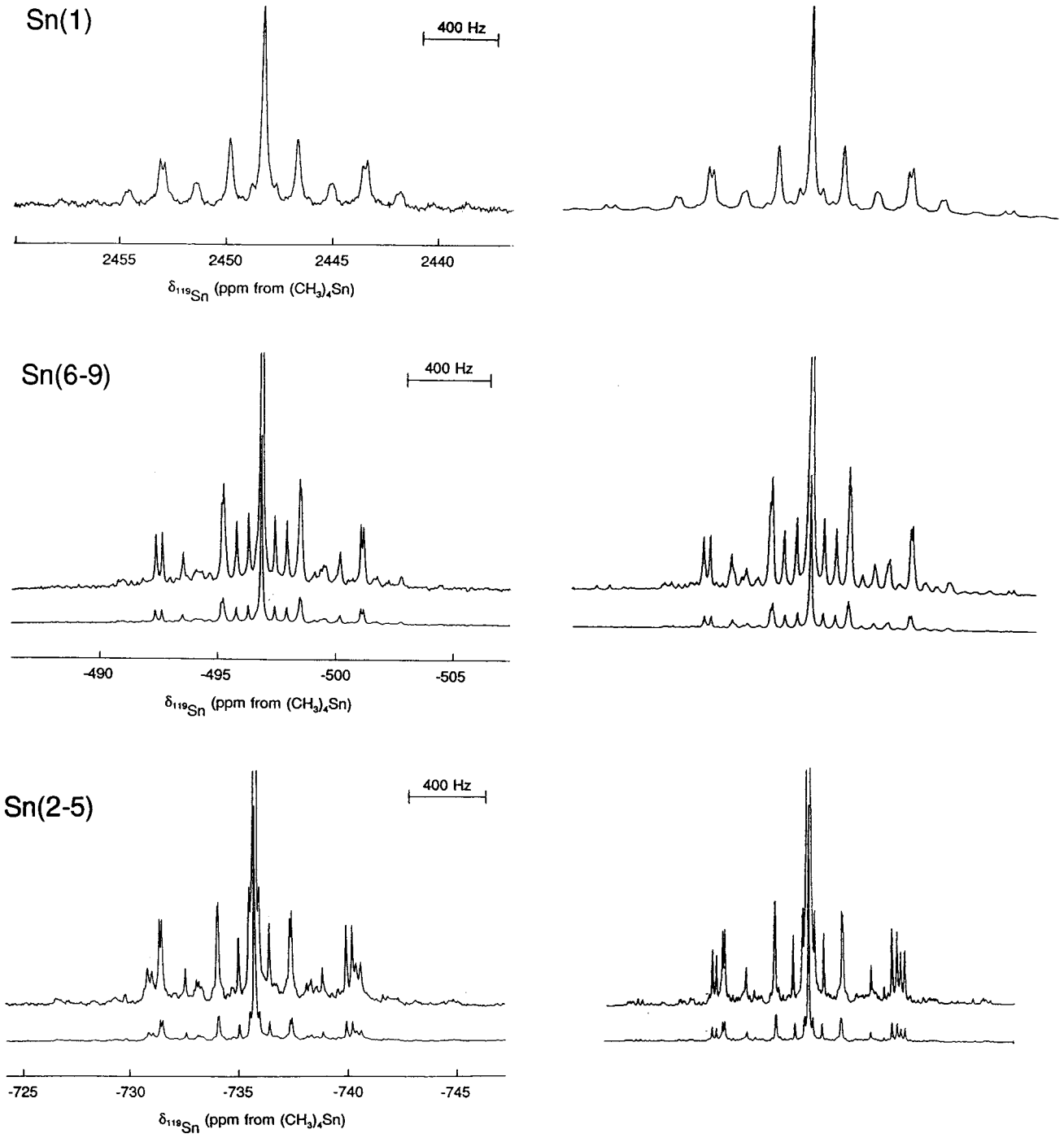

Figure 2. The ^{119}Sn (111.922 MHz) NMR spectra of the Sn(1), Sn(2,3,4,5), and Sn(6,7,8,9) environments in the [1-W(CO)$_3$(η^4-Sn$_9$)]$^{4-}$ anion. Simulated spectra are the right-hand traces.

significantly higher frequency of Sn_9^{4-} (−1287 ppm, NH_3 solvent, −10 °C) and shift progressively to lower frequency relative to Sn_9^{4-} in the series Cr (−50 ppm), Mo (−246 ppm), and W (−276 ppm) (Table 3). The global deshielding accompanying coordination of the open vertex of the Sn_9^{4-} cluster to a zero-electron donor transition metal center is the result of electron transfer from the electron rich Sn_9 cage to the π-acid transition metal center. The aforementioned ^{117}Sn and ^{119}Sn chemical shift trends correlate with the calculated charge delocalizations from the E_9 cages and the charge buildups on the transition metals (see Computational Results). The redistribution of charge is also reflected in the ^{95}Mo chemical shifts of (CO)$_3$Mo·mes (−1918.4 ppm) and [1-Mo(CO)$_3$(η^4-Sn$_9$)]$^{4-}$ (−2002.6 ppm), where ^{95}Mo of the anion is shielded by 84.2 ppm relative to M(CO)$_3$·mes (present as excess reagent in the solution) and is more shielded than the ^{95}Mo resonance of Mo(CO)$_6$ (−1865 ppm).[41] Interestingly, the chemical shift of the apical Sn(1) atom in the Mo derivative is not intermediate with respect to those of the Cr

(41) Vosegaard, T.; Skibsted, J.; Jakobsen, H. J. *J. Phys. Chem.* A **1999**, *103*, 9144.

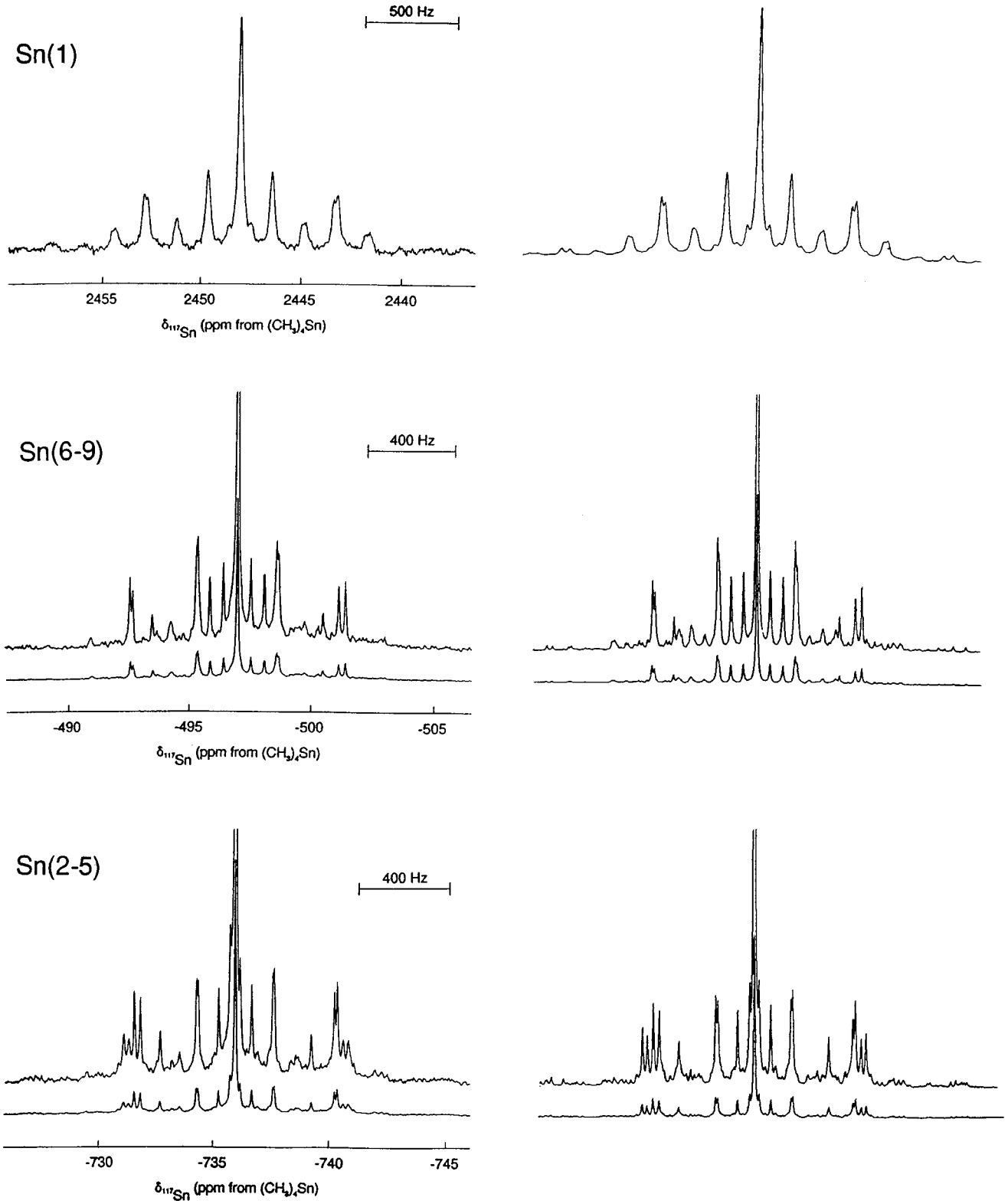

Figure 3. The ^{117}Sn (106.945 MHz) NMR spectra of the Sn(1), Sn(2,3,4,5), and Sn(6,7,8,9) environments in the [1-W(CO)$_3$(η^4-Sn$_9$)]$^{4-}$ anion. Simulated spectra are the right-hand traces.

and W analogues, as was observed for the other two tin resonances, but is significantly more shielded.

(b) Spin−Spin Couplings. The natural abundance ^{117}Sn and ^{119}Sn NMR spectra of the three tin environments of the [1-M(CO)$_3$(η^4-Sn$_9$)]$^{4-}$ anions each display complex ^{117}Sn and ^{119}Sn satellite patterns in addition to intense central lines. The latter arise from the most abundant isotopomer families ^{119}Sn^{0}Sn$_8$M(CO)$_3^{4-}$ and ^{117}Sn^{0}Sn$_8$M(CO)$_3^{4-}$. The most intense satellite patterns are doublet subspectra arising from the J(^{119}Sn−^{119}Sn), J(^{119}Sn−^{117}Sn), and J(^{117}Sn−^{117}Sn) cou-

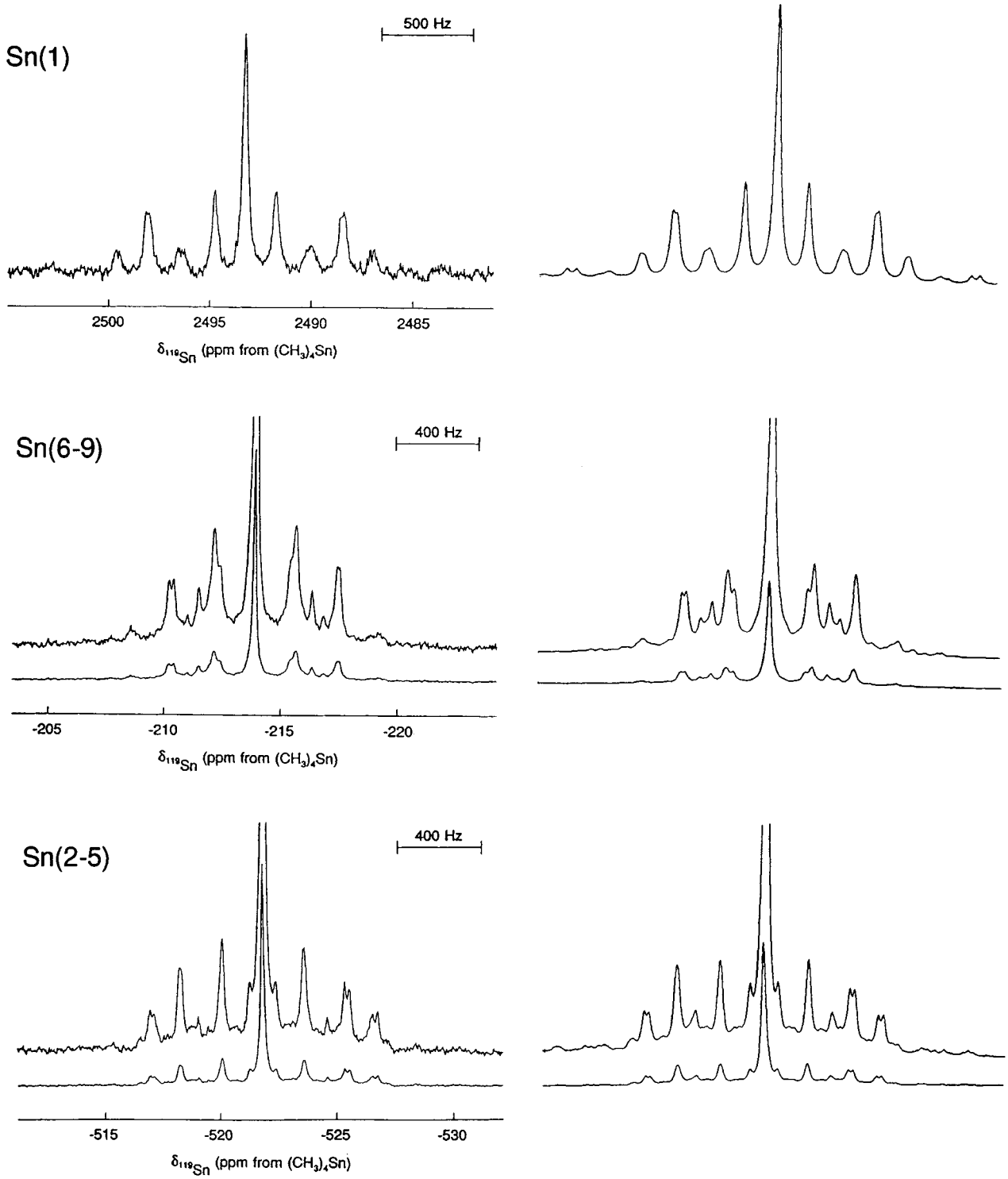

Figure 4. The ^{119}Sn (111.922 MHz) NMR spectra of the Sn(1), Sn(2,3,4,5), and Sn(6,7,8,9) environments in the [1-Cr(CO)$_3$(η^4-Sn$_9$)]$^{4-}$ anion. Simulated spectra are the right-hand traces.

plings of the most abundant isotopomer families, $^{119}Sn_2{}^0Sn_7$-M(CO)$_3{}^{4-}$, $^{119}Sn^{117}Sn^0Sn_7M(CO)_3{}^{4-}$, and $^{117}Sn_2{}^0Sn_7M(CO)_3{}^{4-}$. The next most significant contributors to the satellite spectra are the isotopomer families $^{119}Sn_3{}^0Sn_6M(CO)_3{}^{4-}$, $^{119}Sn_2{}^{117}Sn^0$-$Sn_6M(CO)_3{}^{4-}$, $^{119}Sn^{117}Sn_2{}^0Sn_6M(CO)_3{}^{4-}$, and $^{117}Sn_3{}^0Sn_6$-M(CO)$_3{}^{4-}$, which give rise to weak and more complex subspectra. Tungsten satellite doublets (^{183}W, $I = {}^1/_2$, 14.28% natural abundance) are observed for all three tin environments in the ^{119}Sn and ^{117}Sn NMR spectra of [1-W(CO)$_3$(η^4-Sn$_9$)]$^{4-}$, which arise from the isotopomer families $^{119}Sn^0Sn_8{}^{183}W(CO)_3{}^{4-}$ and $^{117}Sn^0Sn_8{}^{183}W(CO)_3{}^{4-}$.

Two categories of tin−tin spin−spin couplings are distinguishable among the various absolute isotopomers that comprise an isotopomer family, namely, those that arise from intraenvironmental coupling within each Sn$_4$ plane and those that arise from interenvironmental coupling between the Sn$_4$

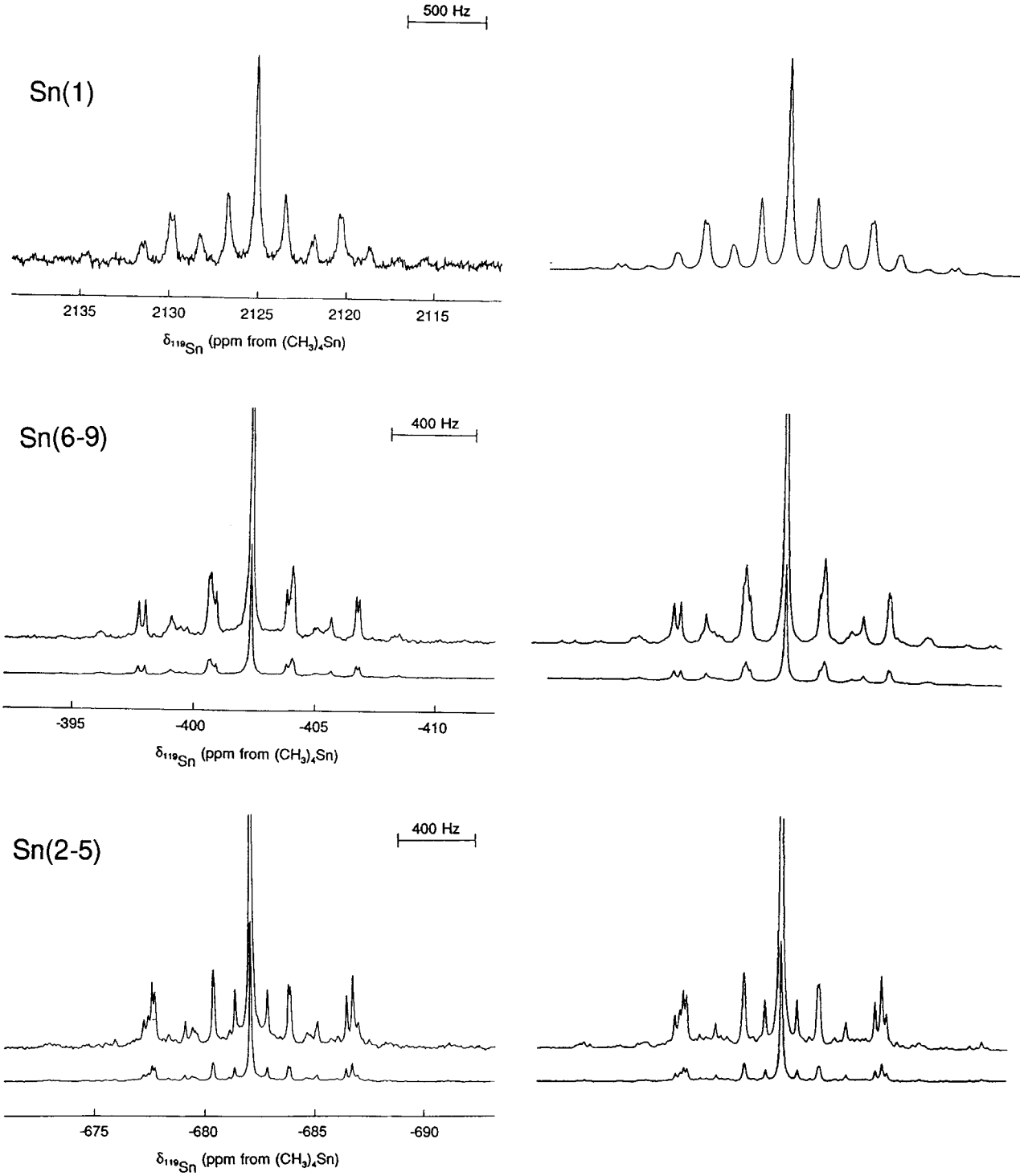

Figure 5. The ^{119}Sn (111.922 MHz) NMR spectra of the Sn(1), Sn(2,3,4,5), and Sn(6,7,8,9) environments in the [1-Mo(CO)$_3$(η^4-Sn$_9$)]$^{4-}$ anion. Simulated spectra are the right-hand traces.

planes or between an Sn_4 plane and the apical tin atom.[42] The ratios $J(^{119}Sn-^{119}Sn)/J(^{119}Sn-^{117}Sn)$ and $J(^{119}Sn-^{117}Sn)/J(^{117}Sn-^{117}Sn)$ (hereafter referred to as R_J) are used to verify the assignment of $^{117}Sn/^{119}Sn$ doublet satellite pairs to the interenvironmental couplings $J(^{119}Sn-^{119}Sn)$, $J(^{119}Sn-^{117}Sn)$, and $J(^{117}Sn-^{117}Sn)$. The R_J ratios are equal to the ratio of the gyromagnetic ratios of the ^{119}Sn and ^{117}Sn nuclides, $\gamma(^{119}Sn)/\gamma(^{117}Sn) = 1.046$ (hereafter referred to as R_γ).[43] In contrast, the intraenvironmental couplings, $J(^{119}Sn-^{117}Sn)$, are observed as single ^{117}Sn satellite doublets in the ^{119}Sn NMR spectrum and as single ^{119}Sn satellites in the ^{117}Sn NMR spectrum. Edge- and diagonal-type intraenvironmental couplings are expected for each plane, e.g., J(Sn(2)−Sn(4)) and J(Sn(2)−Sn(3)) for Sn(2,3,4,5) and J(Sn(6)−Sn(8)) and J(Sn(6)−Sn(7)) for Sn(6,7,8,9). Doublet satellites associated with couplings along diagonal paths are readily assigned, because they are half the intensity of the doublet satellites arising from the edge couplings. The edge couplings typified

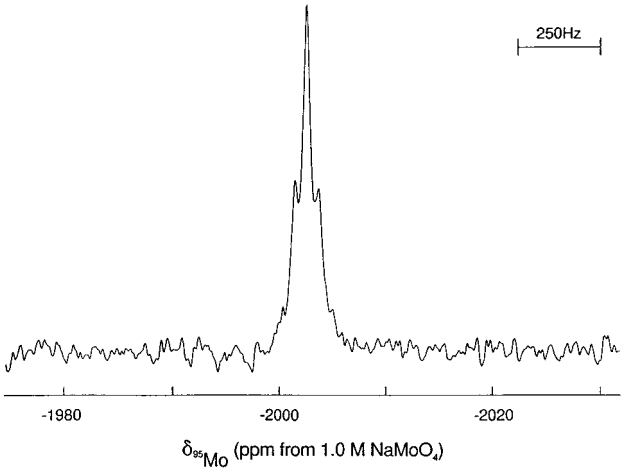

Figure 6. The ^{95}Mo (32.593 MHz) NMR spectrum of the [1-Mo(CO)$_3$-(η^4-Sn$_9$)]$^{4-}$ anion.

by J(Sn(2)−Sn(3)) and J(Sn(6)−Sn(7))[42] were differentiated by their sensitivity to varying M, with the most variation expected for the plane η^4-coordinated to the transition metal. This is also reflected in both the calculated and observed Sn−Sn distances, and in the calculated charges (see Computational Results). The unequivocal assignments of the intraenvironmental couplings allowed for definitive chemical shift assignments of the Sn(2,3,4,5) and Sn(6,7,8,9) planes and of the interenvironmental couplings J(Sn(1)−Sn(2)) and J(Sn(1)−Sn(6)). The assignments of the remaining two interenvironmental couplings, J(Sn(2)−Sn(6)) and J(Sn(2)−Sn(8)), cannot be differentiated, because their associated doublet satellites have the same intensities and the spectral simulation (vide infra) is unable to distinguish between coupling paths having the same symmetry relationships. Within the Sn$_8$ square antiprism, we note that adjacent couplings are smaller [e.g., J(Sn(2)−Sn(3)) and J(Sn(6)−Sn(7))] than couplings whose paths pass through the cluster [e.g., J(Sn(2)−Sn(4)) and J(Sn(6)−Sn(8))]. Accordingly, J(Sn(2)−Sn(6)) and its equivalents[42] have been assigned to the smaller value (Table 4; also see Computational Results, (g) Coupling Constants).

The ^{117}Sn and ^{119}Sn NMR spectra of the [1-M(CO)$_3$(η^4-Sn$_9$)]$^{4-}$ anions were fully assigned based on the above considerations and confirmed using the multinuclear NMR simulation program ISOTOPOMER.[44] Spectra were simulated using the natural abundances of the spin-$^1/_2$ nuclei ^{119}Sn (8.58%) and ^{117}Sn (7.61%) and that of ^{183}W (14.28%)[43] in the case of [1-W(CO)$_3$(η^4-Sn$_9$)]$^{4-}$. In the case of [1-Cr(CO)$_3$(η^4-Sn$_9$)]$^{4-}$ and [1-Mo(CO)$_3$(η^4-Sn$_9$)]$^{4-}$, complete quadrupolar collapse of the transition metal−tin couplings was assumed. Full spectral simulations were achieved by assuming C_{4v} symmetry for the MSn$_9$ cage and required several thousand absolute isotopomers (see Experimental; Simulation of NMR Spectra). The most abundant isotopomers and their subspectra that comprise the ^{119}Sn and ^{117}Sn NMR spectra of the [1-M(CO)$_3$(η^4-Sn$_9$)]$^{4-}$ anions are given in Tables 5 and 6. The simulated spectra are in excellent agreement with the experimental spectra (Figures 2−5), accounting for *all* of the observed spectral features including distortions arising from second-order effects (vide infra) and for *all* coupling paths consistent with the rigid bicapped square antiprismatic geometries of the MSn$_9$ clusters. The complete set of tin−tin spin−spin couplings and their assignments is given in Table 4. Because the spectral analyses for all three [1-M(CO)$_3$-(η^4-Sn$_9$)]$^{4-}$ anions are very similar, only the major isotopomer contributions and their ^{119}Sn and ^{117}Sn subspectra for [1-W(CO)$_3$(η^4-Sn$_9$)]$^{4-}$ are described in detail in the ensuing discussion.

The experimental and simulated ^{119}Sn and ^{117}Sn NMR spectra of the [1-W(CO)$_3$(η^4-Sn$_9$)]$^{4-}$ anion are depicted in Figures 2 and 3. The resonance assigned to the apical Sn(1) (2448.2 ppm) consists of a singlet flanked by ^{183}W satellites [J(^{119}Sn−^{183}W) = 125 Hz] as well as by several sets of ^{119}-Sn and ^{117}Sn satellites. The two most intense sets of symmetrically disposed ^{117}Sn and ^{119}Sn satellites are assigned to the two interenvironmental Sn−Sn couplings. The smaller set of couplings, J(^{119}Sn−^{119}Sn) = 357 Hz, J(^{119}Sn−^{117}Sn) = 342 Hz, and J(^{117}Sn−^{117}Sn) = 335 Hz (R_J = 1.046), is assigned to the coupling between Sn(1) and the nonadjacent basal Sn(6,7,8,9) plane, which is coordinated to the W(CO)$_3$ group, while the larger set of couplings, J(^{119}Sn−^{119}Sn) = 1091 Hz, J(^{119}Sn−^{117}Sn) = 1043 Hz, and J(^{117}Sn−^{117}Sn) = 995 Hz (R_J = 1.046), is assigned to couplings between Sn(1) and the adjacent basal Sn(2,3,4,5) plane. The next most intense satellites result from the doublet-of-doublets subspectra corresponding to the J(^{119}Sn(1)−^{117,119}Sn(2)) doublet whose transitions are further split into a doublet by J(^{119}Sn(1)−^{117,119}Sn(6)).

The ^{117}Sn and ^{119}Sn resonances assigned to the basal Sn(2,3,4,5) plane (−735.7 ppm) and to the middle Sn(6,7,8,9) plane (−496.9 ppm) each consist of a singlet flanked by a set of ^{183}W doublet satellites, J(^{119}Sn−^{183}W) = 47 and 125 Hz and J(^{117}Sn−^{183}W) = 45 and 119 Hz, respectively, and several sets of ^{119}Sn and ^{117}Sn satellites. The ^{119}Sn (^{117}Sn) satellites corresponding to the interenvironmental coupling between the Sn(2,3,4,5) and Sn(6,7,8,9) planes and the apical

(42) With the exception of J(M−Sn(1)), all couplings listed and discussed in the paper represent one of several equivalent coupling paths. These J coupling equivalencies are as follows: J(Sn(1)−Sn(2)) = J(Sn(1)−Sn(3)), J(Sn(1)−Sn(4)), J(Sn(1)−Sn(5)); J(Sn(1)−Sn(6)) = J(Sn(1)−Sn(7)), J(Sn(1)−Sn(8)), J(Sn(1)−Sn(9)); J(Sn(2)−Sn(3)) = J(Sn(3)−Sn(4)), J(Sn(4)−Sn(5)), J(Sn(2)−Sn(5)); J(Sn(2)−Sn(4)) = J(Sn(3)−Sn(5)); J(Sn(6)−Sn(7)) = J(Sn(7)−Sn(8)), J(Sn(8)−Sn(9)), J(Sn(6)−Sn(9)); J(Sn(6)−Sn(8)) = J(Sn(7)−Sn(9)); J(Sn(2)−Sn(6)) = J(Sn(2)−Sn(9)), J(Sn(3)−Sn(7)), J(Sn(3)−Sn(6)), J(Sn(4)−Sn(8)), J(Sn(4)−Sn(7)), J(Sn(5)−Sn(8)), J(Sn(5)−Sn(9)); J(Sn(2)−Sn(8)) = J(Sn(2)−Sn(7)), J(Sn(3)−Sn(8)), J(Sn(3)−Sn(9)), J(Sn(4)−Sn(6)), J(Sn(4)−Sn(9)), J(Sn(5)−Sn(7)), J(Sn(5)−Sn(6)); J(M−Sn(2)) = J(M−Sn(3)), J(M−Sn(4)), J(M−Sn(5)); J(M−Sn(6)) = J(M−Sn(7)), J(M−Sn(8)), J(M−Sn(9)). These equivalencies were also used for averaging the bond lengths and bond orders given in Table 7.

(43) Mason, J. In *Multinuclear NMR*; Mason, J., Ed.; Plenum Press: New York, 1987; Appendix, pp 626−628.

(44) Santry, D. P.; Mercier, H. P. A.; Schrobilgen, G. J. *ISOTOPOMER, A Multi-NMR Simulation Program*, version 3.02NTF.; Snowbird Software, Inc.: Hamilton, ON, Canada, 2000.

(45) Emsley, J. W.; Feeney, J.; Sutcliffe, L. H. *High-Resolution Nuclear Magnetic Resonance Spectroscopy*, Pergamon Press: London, 1965; Vol. 1, Chapter 8, pp 310−320.

(46) Gay, I. D.; Jones, C. H. W.; Sharma, R. D. *J. Magn. Reson.* **1989**, *84*, 501.

(47) Kennedy, J. D.; McFarlane, W. *J. Chem. Soc., Dalton Trans.* **1976**, 1219.

Table 3. Calculated[a] and Experimental[b] Tin NMR Chemical Shifts (ppm) for Sn_9^{4-} and $[1\text{-}M(CO)_3(\eta^4\text{-}Sn_9)]^{4-}$ (M = Cr, Mo, W) Anions

	Sn_9^{4-}		$Sn_9Cr(CO)_3^{4-}$		$Sn_9Mo(CO)_3^{4-}$		$Sn_9W(CO)_3^{4-}$	
atom(s)[c]	GIAO	expt	GIAO	expt	GIAO	expt	GIAO	expt
Sn(1)	−530		3069	2493.2	2666	2125.1	2727	2448.2
Sn(2,3,4,5)	−272		655	−521.9	543	−682.1	440	−735.7
Sn(6,7,8,9)	−608		592	−213.9	539	−402.4	487	−496.9
Sn(1−9)[d]	−450	−1291.9	895	−50.0	777	−245.9	715	−275.8

[a] Calculated chemical shifts are given relative to $Sn(CH_3)_4$ (2934 ppm). [b] Values obtained from the ^{117}Sn and ^{119}Sn NMR spectra recorded at 0 °C in liquid NH_3. [c] The cluster numbering schemes are given in Figure 1. [d] Average chemical shifts.

Table 4. Spin−Spin Coupling Constants (Hz) for the $[1\text{-}M(CO)_3(\eta^4\text{-}Sn_9)]^{4-}$ (M = Cr, Mo, W) Anions[a,b]

	intraenvironmental $J(^{117,119}Sn-^{117,119}Sn)$, Hz			
anion	Sn(2)−Sn(3)	Sn(2)−Sn(4)	Sn(6)−Sn(7)	Sn(6)−Sn(8)
$Sn_9Cr(CO)_3^{4-}$	129	621	544	656
$Sn_9Mo(CO)_3^{4-}$	165	673	324	739
$Sn_9W(CO)_3^{4-}$	154	700	238	745

	interenvironmental $J(^{117,119}Sn-^{117,119}Sn)$, Hz			
anion	Sn(1)−Sn(2)	Sn(1)−Sn(6)	Sn(2)−Sn(6)	Sn(2)−Sn(8)
$Sn_9Cr(CO)_3^{4-}$	1048	328	393	783
	[1098]	[342]		[821]
$Sn_9Mo(CO)_3^{4-}$	1042	351	375	975
	[1091]	[367]	[391]	[1021]
$Sn_9W(CO)_3^{4-}$	1043	342	363	943
	(995)	(335)	(348)	(901)
	[1091]	[357]	[378]	[985]

	interenvironmental $J(^{119}Sn-M)$, Hz			
anion	Sn(1)−M	Sn(2)−M	Sn(6)−M	
$Sn_9Mo(CO)_3^{4-}$	75[c]		75[c]	(M = ^{95}Mo)
$Sn_9W(CO)_3^{4-}$	125	47	125	(M = ^{183}W)
	(116)	(45)	(119)	

[a] The numbering scheme is given in Figure 1. [b] Values denote $J(^{119}Sn-^{117}Sn)$, whereas values in parentheses denote $J(^{117}Sn-^{117}Sn)$ or $J(^{117}Sn-^{183}W)$ in the case of $Sn_9W(CO)_3^{4-}$ and those in square brackets denote $J(^{119}Sn-^{119}Sn)$. [c] Values are the unresolved ^{117}Sn and ^{119}Sn satellites on the ^{95}Mo resonance at $\delta(^{95}Mo) = -2002.6$ ppm (30 °C).

Sn(1) atom are also symmetrically disposed about the central line in the ^{117}Sn (^{119}Sn) spectrum. However, the ^{119}Sn (^{117}Sn) satellites corresponding to the two interenvironmental coupling paths between the two Sn_4-planes, e.g., Sn(2)−Sn(6) and Sn(2)−Sn(8),[42] do not symmetrically flank the central line in the ^{119}Sn (^{117}Sn) spectrum. The R_J ratios for these interenvironmental couplings [1.041 for Sn(2)−Sn(6) and 1.045 for Sn(2)−Sn(8)] are in excellent agreement with R_γ. The centroids of satellites arising from $J(^{119}Sn(2)-^{119}Sn(6))$ = 378 Hz, ($J(^{117}Sn(2)-^{117}Sn(6))$ = 348 Hz) and $J(^{119}Sn(2)-^{119}Sn(8))$ = 985 Hz ($J(^{117}Sn(2)-^{117}Sn(8))$ = 901 Hz) are shifted relative to the central line of each environment, and to high frequency and to low frequency by 1.2 and 8.8 (0.8 and 7.7) Hz for the Sn(6,7,8,9) and Sn(2,3,4,5) environments, respectively, in the ^{119}Sn (^{117}Sn) spectrum. These asymmetries arise because the magnitudes of $J(^{119}Sn(2)-^{119}Sn(6))$ ($J(^{117}Sn(2)-^{117}Sn(6))$) and $J(^{119}Sn(2)-^{119}Sn(8))$ ($J(^{117}Sn(2)-^{117}Sn(8))$) are a significant percentage of the frequency difference between the Sn(2,3,4,5) and Sn(6,7,8,9) environments, $\nu_o\delta$ = 26 736 (25 557) Hz in the ^{119}Sn (^{117}Sn) spectrum, yielding $J/\nu_o\delta$ ratios of 0.0141 (0.0136) and 0.0368 (0.0353), respectively, and are attributed to second-order effects that give rise to weakly coupled AB spin systems.[45] Consequently, the ^{119}Sn (^{117}Sn) satellites in the ^{119}Sn (^{117}Sn) spectrum having $J/\nu_o\delta$ = 0.0368 (0.0353) exhibit a more severe second-order perturbation than those having $J/\nu_o\delta$ = 0.0141 (0.0136). Similar second-order effects are noted for the Cr and Mo analogues, and more severe second-order effects have been observed in the ^{119}Sn NMR spectra of the $Sn[Sn(CH_3)]_3^-$ anion [$\nu_o\delta$ = 20 950 Hz, $J(^{119}Sn-^{119}Sn)$ = 5185 Hz, $J/\nu_o\delta = 0.25$][46] and $((CH_3)_2SnS)_3$ [$\nu_o\delta$ = 388 Hz, $J(^{119}Sn-^{119}Sn)$ = 198 Hz, $J/\nu_o\delta = 0.51$].[47]

The experimental and simulated ^{119}Sn and ^{117}Sn NMR spectra of the chromium and molybdenum clusters (Figures 4 and 5) are very similar to those of the $[1\text{-}W(CO)_3(\eta^4\text{-}Sn_9)]^{4-}$ anion but are somewhat broader, with the line widths being broadest for the Cr anion (see Experimental; Simulation of NMR Spectra). The second-order effects observed for the ^{117}Sn and ^{119}Sn resonances of the Sn_4 planes of $[1\text{-}W(CO)_3(\eta^4\text{-}Sn_9)]^{4-}$ are also evident for the tin resonances of the chromium and molybdenum analogues; however, the broad line widths of the ^{119}Sn and ^{117}Sn resonances of $[1\text{-}Cr(CO)_3(\eta^4\text{-}Sn_9)]^{4-}$ preclude observation of these effects for the smaller Sn(2)−Sn(6) type interenvironmental couplings. Although Mo and Cr possess quadrupolar isotopes (^{95}Mo, I = 5/2, 15.72% natural abundance; ^{97}Mo, I = 5/2, 9.46% natural abundance; ^{53}Cr, I = 3/2, 9.55% natural abundance),[43] the broader line widths are not attributable to quadrupolar relaxation, because the natural abundances of these nuclides are too low. The line widths of the Cr and Mo anions showed no significant variation when recorded at 30, 0, and −70 °C or at different field strengths (7.046 and 11.744 T), thus apparently ruling out exchange and relaxation by quadrupolar[48] and CSA (chemical shift anisotropy)[49] mechanisms.

The ^{95}Mo NMR spectrum of $[1\text{-}Mo(CO)_3(\eta^4\text{-}Sn_9)]^{4-}$ was obtained at 30 °C in liquid NH_3 (Figure 6) and consists of a singlet (−2002.6 ppm) flanked by $^{117,119}Sn$ satellites [$J(^{95}Mo-^{117,119}Sn)$ = 75 Hz] for which the individual ^{117}Sn and ^{119}Sn components were not resolved. Inability to observe the ^{95}Mo satellites in the ^{117}Sn and ^{119}Sn spectra at 30 °C and the observation of only a single set of $^{117,119}Sn$ satellites prevented assignment of the $J(^{95}Mo-^{117,119}Sn)$ coupling to a specific coupling path. However, the $J(^{183}W-^{119}Sn)$ and $J(^{183}W-^{117}Sn)$ couplings corresponding to coupling between tungsten and the apical Sn(1) atom and between tungsten and the Sn(6,7,8,9) ring have been assigned in their respective ^{117}Sn and ^{119}Sn spectra and are essentially equal in magnitude. It is therefore reasonable to assign $J(^{95}Mo-^{117,119}Sn)$ = 75 Hz

(48) Howarth, O. In *Multinuclear NMR*; Mason, J., Ed.; Plenum Press: New York, 1987; Chapter 5, pp 150−152.
(49) Howarth, O. In *Multinuclear NMR*; Mason, J., Ed.; Plenum Press: New York, 1987; Chapter 5, p 149.

Table 5. The Most Abundant Isotopomers and Subspectra Comprising the ^{119}Sn and ^{117}Sn NMR Spectra of the [1-W(CO)$_3$(η^4-Sn$_9$)]$^{4-}$ Anion

^{119}Sn$_x$^{117}Sn$_y$^{0}Sn$_{9-x-y}$-^{183}W$_z$W$_{1-z}$[a]					multiplicity[b] apical Sn(1)		^{119}Sn$_x$^{117}Sn$_y$^{0}Sn$_{9-x-y}$-^{183}W$_z$W$_{1-z}$[a]					multiplicity[b] Sn(2−5) belt		^{119}Sn$_x$^{117}Sn$_y$^{0}Sn$_{9-x-y}$-^{183}W$_z$ W$_{1-z}$[a]					multiplicity[b] Sn(6−9) belt	
x	y	z	^{119,117}Sn environ	fractional isotopomer abundance[a]	^{119}Sn	^{117}Sn	x	y	z	^{119,117}Sn environ	fractional isotopomer abundance[a]	^{119}Sn	^{117}Sn	x	y	z	^{119,117}Sn environ	fractional isotopomer abundance[a]	^{119}Sn	^{117}Sn
1	0	0	(1)	0.0179	S	−	1	0	0	(2−5)	0.0716	S	−	1	0	0	(6−9)	0.0716	S	−
1	0	1	(1)	0.0030	d_{11}	−	1	0	1	(2−5)	0.0119	d_{10}	−	1	0	1	(6−9)	0.0119	d_9	−
1	1	0	(1, 2−5)	0.0065	d_1	d_1''	1	1	0	(1,2−5)	0.0065	d_1	d_1''							
1	1	0	(1, 6−9)	0.0065	d_2	d_2''								1	1	0	(1,6−9)	0.0065	d_2	d_2''
							1	1	0	(2,6)	0.0260	d_3	d_3''	1	1	0	(2,6)	0.0260	d_3	d_3''
							1	1	0	(2,8)	0.0260	d_4	d_4''	1	1	0	(2,8)	0.0260	d_4	d_4''
							1	1	0	(2,3)	0.0130	d_5	d_5''	1	1	0	(6,7)	0.0130	d_7	d_7''
							1	1	0	(2,4)	0.0065	d_6	d_6''	1	1	0	(6,8)	0.0065	d_8	d_8''
2	0	0	(1, 2−5)	0.0073	d_1'	-	2	0	0	(1,2−5)	0.0073	d_1'	−							
2	0	0	(1, 6−9)	0.0073	d_2'	-								2	0	0	(1,6−9)	0.0073	d_2'	−
							2	0	0	(2,6)	0.0147	d_3'	−	2	0	0	(2,6)	0.0147	d_3'	−
							2	0	0	(2,8)	0.0147	d_4'	−	2	0	0	(2,8)	0.0147	d_4'	−
							2	0	0	(2,3)	0.0073	d_5'	−	2	0	0	(6,7)	0.0073	d_7'	−
							2	0	0	(2,4)	0.0037	d_6'	−	2	0	0	(6,8)	0.0037	d_8'	−
0	1	0	(1)	0.0159	−	S	0	1	0	(2,5)	0.0635	−	S	1	0	0	(6−9)	0.0635	−	S
0	1	1	(1)	0.0026	−	d_{11}''	0	1	1	(2,5)	0.0106	−	d_{10}''	1	0	1	(6−9)	0.0106	−	d_9''
0	2	0	(1, 2−5)	0.0058	−	d_1''	0	2	0	(1,2−5)	0.0058	−	d_1''							
0	2	0	(1, 6−9)	0.0058	−	d_2''								0	2	0	(1,6−9)	0.0058	−	d_2''
							0	2	0	(2,6)	0.0115	−	d_3''	0	2	0	(2,6)	0.0115	−	d_3''
							0	2	0	(2,8)	0.0115	−	d_4''	0	2	0	(2,8)	0.0115	−	d_4''
							0	2	0	(2,3)	0.0058	−	d_5''	0	2	0	(6,7)	0.0058	−	d_7''
							0	2	0	(2,4)	0.0029	−	d_6''	0	2	0	(6,8)	0.0029	−	d_8''

[a] Natural abundances of the spin-$^1/_2$ nuclides used to calculate isotopomer abundances were taken from ref 43: ^{117}Sn, 7.61%; ^{119}Sn, 8.58%; ^{183}W, 14.28%. The natural abundance of ^{115}Sn (0.35%) is too low to contribute detectable isotopomer subspectra and is combined with the spinless tin nuclides. [b] S denotes a singlet; d denotes a doublet arising from J(^{119}Sn−^{117}Sn) or J(^{119}Sn−^{183}W); d′ denotes a doublet arising from J(^{119}Sn−^{119}Sn); d″ denotes a doublet arising from J(^{117}Sn−^{117}Sn) or J(^{117}Sn−^{183}W). The right-hand subscript on d, d′, and d″ denotes the coupling path, i.e., 1 = J(Sn(1)−Sn(2)), 2 = J(Sn(1)−Sn(6)), 3 = J(Sn(2)−Sn(6)), 4 = J(Sn(2)−Sn(8)), 5 = J(Sn(2)−Sn(3)), 6 = J(Sn(2)−Sn(4)), 7 = J(Sn(6)−Sn(7)), 8 = J(Sn(6)−Sn(8)), 9 = J(Sn(6)−W), 10 = J(Sn(2)−W), 11 = J(Sn(1)−W). With the exception of J(Sn(1)−W), each of the designated couplings represents two or more equivalent coupling paths (see ref 42).

Table 6. The Most Abundant Isotopomers and Subspectra Comprising the ^{119}Sn and ^{117}Sn NMR Spectra of the [1-M(CO)$_3$(η^4-Sn$_9$)]$^{4-}$ Anions Where (M = Cr, Mo) (see Table 5 for footnotes)

^{119}Sn$_x$^{117}Sn$_y$^{0}Sn$_{9-x-y}$M[a]			fractional isotopomer abundance[a]	multiplicity[b] apical Sn(1)		^{119}Sn$_x$^{117}Sn$_y$^{0}Sn$_{9-x-y}$M[a]			fractional isotopomer abundance[a]	multiplicity[b] Sn(2−5) belt		^{119}Sn$_x$^{117}Sn$_y$^{0}Sn$_{9-x-y}$M[a]			fractional isotopomer abundance[a]	multiplicity[b] Sn(6−9) belt	
x	y	^{119,117}Sn environ		^{119}Sn	^{117}Sn	x	y	^{119,117}Sn environ		^{119}Sn	^{117}Sn	x	y	^{119,117}Sn environ		^{119}Sn	^{117}Sn
1	0	(1)	0.0209	S	−	1	0	(2−5)	0.0835	S	−	1	0	(6−9)	0.0835	S	−
1	1	(1,2−5)	0.0076	d_1	d_1''	1	1	(1,2−5)	0.0076	d_1	d_1''						
1	1	(1,6−9)	0.0076	d_2	d_2''							1	1	(1,6−9)	0.0076	d_2	d_2''
						1	1	(2,6)	0.0152	d_3	d_3''	1	1	(2,6)	0.0152	d_3	d_3''
						1	1	(2,8)	0.0152	d_4	d_4''	1	1	(2,8)	0.0152	d_4	d_4''
						1	1	(2,3)	0.0152	d_5	d_5''	1	1	(6,7)	0.0152	d_7	d_7''
						1	1	(2,4)	0.0076	d_6	d_6''	1	1	(6,8)	0.0076	d_8	d_8''
2	0	(1,2−5)	0.0086	d_1'	−	2	0	(1,2−5)	0.0086	d_1'	−						
2	0	(1,6−9)	0.0086	d_2'	−							2	0	(1,6−9)	0.0086	d_2'	−
						2	0	(2,6)	0.0171	d_3'	−	2	0	(2,6)	0.0171	d_3'	−
						2	0	(2,8)	0.0171	d_4'	−	2	0	(2,8)	0.0171	d_4'	−
						2	0	(2,3)	0.0086	d_5'	−	2	0	(6,7)	0.0086	d_7'	−
						2	0	(2,4)	0.0043	d_6'	−	2	0	(6,8)	0.0043	d_8'	−
0	1	(1)	0.0185	−	S	0	1	(2−5)	0.0741	−	S	1	0	(6−9)	0.0741	−	S
0	2	(1,2−5)	0.0067	−	d_1''	0	2	(1,2−5)	0.0067	−	d_1''						
0	2	(1,6−9)	0.0067	−	d_2''							0	2	(1,6−9)	0.0067	−	d_2''
						0	2	(2,6)	0.0135	−	d_3''	0	2	(2,6)	0.0135	−	d_3''
						0	2	(2,8)	0.0135	−	d_4''	0	2	(2,8)	0.0135	−	d_4''
						0	2	(2,3)	0.0067	−	d_5''	0	2	(6,7)	0.0067	−	d_7''
						0	2	(2,4)	0.0034	−	d_6''	0	2	(6,8)	0.0034	−	d_8''

to one or both of the analogous coupling paths in [1-Mo(CO)$_3$(η^4-Sn$_9$)]$^{4-}$.

Characterization of the [1-Mo(CO)$_3$(η^4-Pb$_9$)]$^{4-}$ Anion by NMR Spectroscopy. Solutions obtained from the reactions of Mo(CO)$_3$·mes with Pb$_9^{4-}$ are unstable over the periods of time required for acquisition of the ^{207}Pb NMR spectra in en and liquid NH$_3$, decomposing to give emerald green NH$_3$ solutions characteristic of the paramagnetic Pb$_9^{3-}$ anion,[13] lead mirrors, and pale yellow en solutions. The reaction of Pb$_9^{4-}$ with Mo(CO)$_3$·mes in en initially gave a red-brown solution and led to the observation of two broad, equally intense ^{207}Pb resonances at −1869 ppm ($\Delta\nu_{1/2}$ = 1200 Hz) and −3100 ppm ($\Delta\nu_{1/2}$ = 990 Hz). Each resonance was accompanied by a broad satellite doublet corresponding to J(^{207}Pb−^{207}Pb) ≈ 4500 Hz and is respectively assigned to the Pb(6,7,8,9) and Pb(2,3,4,5) planes of the [1-Mo(CO)$_3$(η^4-Pb$_9$)]$^{4-}$ anion by analogy with the tin chemical shift assignments for the [1-M(CO)$_3$(η^4-Sn$_9$)]$^{4-}$ anions (see Char-

acterization of the [1-M(CO)$_3$(η^4-Sn$_9$)]$^{4-}$ (M = Cr, Mo, W) Anions by NMR Spectroscopy, (a)). Unfortunately, the rapid decomposition of these solutions prevented the observation of the apical Pb(1) atom resonance. Samples prepared in liquid NH_3 and recorded at −70 °C, however, yielded three resonances having considerably narrower line widths (Figure S3). The two low-frequency resonances also displayed well-resolved ^{207}Pb satellites, with two satellite doublets appearing on the higher frequency resonance, i.e., −1934 ppm ($\Delta\nu_{1/2}$ = 230; J(^{207}Pb−^{207}Pb) = 660 and 4630 Hz) and −3450 ppm ($\Delta\nu_{1/2}$ = 200 Hz; J(^{207}Pb−^{207}Pb) = 4580 Hz). Although the chemical shifts of the latter resonances are significantly shifted to lower frequency relative to those in en at room temperature, they are readily assigned to the pair of resonances observed at room temperature in en solution based on their satellite couplings. The sensitivity of the chemical shifts to temperature and solvent is not unexpected, as these effects have been shown to be large for a number of heavy NMR nuclides.[50] The third resonance at 27 ppm ($\Delta\nu_{1/2}$ = 250 Hz), assigned to Pb(1), does not display resolved satellites but does show pronounced broadening near its base, which is consistent with an unresolved pair of satellites corresponding to that observed on the resonance assigned to the Pb(6,7,8,9) plane (J(^{207}Pb−^{207}Pb) = 660 Hz). The observation of two of the four interenvironmental ^{207}Pb−^{207}Pb couplings expected for a rigid [1-Mo(CO)$_3$(η^4-Pb$_9$)]$^{4-}$ anion establish that the fluxionality of the Pb$_9$ moiety has been modified. The most likely assignments for the observed couplings are to apical−adjacent plane coupling, J(^{207}Pb(1)−^{207}Pb(2)) = 660 Hz, and to the interplanar coupling, J(^{207}Pb-(2)−^{207}Pb(8)) = 4580/4630 Hz. By analogy with the tin anions, the two remaining interplanar couplings are expected to be less than 660 Hz and are presumably not resolved because of broad line widths. Alternatively, the Pb$_4$ planes may be rotating relative to each other and rapidly enough on the NMR time scale to average the two interplanar couplings to a single coupling. The broad line widths in liquid NH_3 at −70 °C may, in part, also arise from spin−lattice relaxation arising from the CSA (chemical shift anisotropy) mechanism.[48] It seems likely that the resonances of the Pb$_4$ planes are further broadened in en solution at 0 °C as a result of additional chemical exchange processes that may be dissociative in nature followed by rapid rearrangement of the Pb$_9$ cluster and/or involve intraanion migration of the Mo center from an η^4-apical position to an η^5-position in a belt with concomitant migration of a Pb atom to an apical position. The latter rearrangement has been proposed by Rudolph[51] and Eichhorn.[20]

Computational Results. (a) Geometries and Bond Orders. The fully optimized geometries show that the E$_9^{4-}$ anions have C_{4v} symmetry and are based on monocapped square antiprisms consistent with PSEPT. The M(CO)$_3$ groups η^4-bonded to the nido-faces of the E$_9^{4-}$ anions in the optimized gas-phase structures. In all cases for the M(CO)$_3$ complexes, no symmetry was used in the calculation. While the Mo/Sn and Cr/Pb anions optimized as C_1 symmetry, the remaining anions optimized as C_s symmetry.

The calculated distances are in good agreement with the experimental ones, although they are all longer by 0.10−0.15 Å than in the experimental structures of the E$_9^{4-}$ and [1-M(CO)$_3$(η^4-E$_9$)]$^{4-}$ anions (Table 7 and also see Supporting Information). The fact that the calculated bond distances are longer than the experimental ones is consistent with our previous results for Pb$_9^{4-}$.[13] The calculated M−E distances are in better agreement with experiment than the E−E distances. Both families of clusters have comparable bond distances, with those of the Sn clusters being slightly shorter than those of the Pb clusters, as expected. The trends observed experimentally upon coordination of the M(CO)$_3$ group are reproduced, i.e., the distances within the basal ring η^4-coordinated to the transition metal expand while those in the middle ring contract (see Structural Characterization by X-ray Crystallography). This is paralleled by increases and decreases in the bond orders, respectively (Table 7). The bond order increases are surprisingly large considering the change of less than 0.1 Å for these distances (<3% of the bond distance). As shown by the bond orders, the interactions within the E(2,3,4,5) ring are somewhat weaker than the interactions between this ring and the apical E(1) atom as well as between this ring and the E(6,7,8,9) ring.

Coordination of the transition metal leads to overall reductions in the E−E bond orders relative to those of the E$_9^{4-}$ anions, and as expected, those of the basal ring are most affected. The E(6,7,8,9) ring bond orders decrease so that they are lower than the E(1)−E(2,3,4,5) bond orders by ∼0.1, but they are still larger than the bond orders in the E(2,3,4,5) ring. The bond orders between diagonal pairs of E atoms are essentially zero in the basal E(6,7,8,9) ring, in contrast with the diagonal bond orders in the E(2,3,4,5) ring. There is a weak interaction between the apical E(1) atom and the transition metal atom of 0.07−0.08 (Sn) and 0.06−0.15 (Pb) and another weak interaction between the middle ring and the transition metal, which increases from 0.06 (Sn) and 0.04 (Pb) for Cr, to 0.16 (Sn) and 0.15 (Pb) for Mo, and to 0.14 (Sn) and 0.16 (Pb) for W. The bond orders between the basal ring and the transition metal show a significant increase from Cr (0.50, Sn; 0.44, Pb) to Mo (0.74, Sn; 0.58, Pb) and W (0.78 Sn; 0.65, Pb). The interactions of the metal with the Pb$_9$ cluster are smaller for Cr and W than with the Sn$_9$ cluster but are comparable for the Mo cluster.

(b) Charges and Valencies. For the E$_9^{4-}$ anions, the apical atoms charges are the most negative followed by the E(6,7,8,9) rings of their nido-faces, with slightly larger charges on the apical atoms (Table 7). The Mayer valencies range from 2.88 to 2.90 for Sn$_9^{4-}$ and from 2.92 to 3.00 for Pb$_9^{4-}$. Bonding of the M(CO)$_3$ group to the nido-face of an E$_9^{4-}$ anion leads to a significant change in the electron populations, with significant delocalization of charge from the E$_9^{4-}$ cluster onto the M(CO)$_3$ group. The largest change is calculated for the basal ring that binds to the transition metal. For Cr, this ring has charges of −0.13 (Sn) and −0.25 (Pb) on each of the E(6,7,8,9) atoms. In the case of tin, the basal ring atom charges for Mo (+0.03) and W (+0.04) are

(50) Brevard, C.; Granger, P. In *Handbook of High-Resolution Multinuclear NMR*, John Wiley & Sons: 1981; p 40.
(51) Pretzer, W. R.; Rudolph, R. W. *J. Am. Chem. Soc.* **1976**, *98*, 1441.

Table 7. Calculated Bond Distances, Mayer Bond Orders, Mulliken Charges and Mayer Valencies in the E_9^{4-} and [1-M(CO)$_3$(η^4-E$_9$)]$^{4-}$ Anions (E = Sn, Pb; M = Cr, Mo, W)[a]

	Sn_9^{4-}	$Sn_9Cr(CO)_3^{4-}$	$Sn_9Mo(CO)_3^{4-}$	$Sn_9W(CO)_3^{4-}$	Pb_9^{4-}	$Pb_9Cr(CO)_3^{4-}$	$Pb_9Mo(CO)_3^{4-}$	$Pb_9W(CO)_3^{4-}$	
				Bond Distances and Bond Orders					
E(1)−E(2)	3.113 [0.60]	3.117 [0.55]	3.114 [0.56]	3.112 [0.56]	3.21 [0.64]	3.196 [0.61]	3.20 [0.56]	3.199 [0.61]	
E(1)−E(6)	[0.13]	[0.11]	[0.10]	[0.10]	[0.11]	[0.10]	[0.10]	[0.09]	
E(1)−M		[0.07]	[0.08]	[0.08]		[0.15]	[0.08]	[0.06]	
E(2)−E(3)	3.420 [0.35]	3.352 [0.44]	3.382 [0.41]	3.378 [0.42]	3.50 [0.36]	3.419 [0.47]	3.437 [0.46]	3.437 [0.46]	
E(2)−E(4)	4.84 [0.11]	4.74 [0.11]	4.78 [0.11]	4.78 [0.11]	4.94 [0.07]	4.84 [0.07]	4.86 [0.06]	4.86 [0.06]	
E(2)−E(6)	3.133 [0.60]	3.146 [0.52]	3.133 [0.51]	3.132 [0.50]	3.23 [0.63]	3.233 [0.54]	3.236 [0.51]	3.232 [0.48]	
E(2)−E(8)	[0.14]	[0.09]	[0.09]	[0.09]	[0.11]	[0.06]	[0.05]	[0.05]	
E(2−5)−M		[0.06]	[0.16]	[0.14]		[0.04]	[0.15]	[0.16]	
E(6)−E(7)	3.134 [0.66]	3.196 [0.50]	3.229 [0.45]	3.239 [0.43]	3.24 [0.69]	3.266 [0.57]	3.297 [0.52]	3.303 [0.48]	
E(6)−E(8)[b]	4.43	4.52	4.56	4.58	4.58	4.62	4.66	4.67	
E(6)−M		2.935 [0.50]	3.068 [0.74]	3.079 [0.78]		3.025 [0.44]	3.155 [0.58]	3.155 [0.65]	
M−C		1.42	1.33	1.35		1.49	1.34	1.38	
M−O		0.14	0.27	0.26		0.16	0.29	0.27	
C−O		2.00	1.86	1.85		1.97	1.81	1.80	
C−C		0.07	0.11	0.09		0.08	0.10	0.08	
				Charges					
E(1)	−0.529	−0.423	−0.399	−0.398	−0.591	−0.485	−0.459	−0.457	
E(2−5)	−0.397	−0.370	−0.350	−0.358	−0.365	−0.336	−0.350	−0.360	
E(6−9)	−0.474	−0.130	+0.026	+0.042	−0.488	−0.246	−0.060	−0.018	
M		−0.950	−1.267	−1.185		−0.503	−0.668	−0.717	
C		+0.106	−0.018	−0.054		+0.110	−0.069	−0.093	
O		−0.323	−0.327	−0.330		−0.339	−0.341	−0.345	
		+1.376	+2.000	+2.064		+0.968	+1.712	+1.880	Δ(6−9)[c]
		+1.597	+2.305	+2.338		+1.187	+1.901	+2.031	Δ(1−9)[c]
				Valencies					
E(1)	2.894	2.768	2.755	2.755	3.001	2.926	2.912	2.912	
E(2−5)	2.882	2.861	2.855	2.853	2.924	2.892	2.914	2.915	
E(6−9)	2.903	2.932	3.041	3.030	2.960	2.939	2.987	2.970	
M		6.989	8.470	8.584		6.884	7.864	8.261	
C		3.768	3.620	3.577		3.763	3.646	3.581	
O		2.251	2.226	2.218		2.226	2.198	2.191	

[a] For simplicity, and because the E$_9$ unit is very close to C_{4v} point symmetry in all the anions, only average values are given. A full listening can be found in Tables S1 and S2 of the Supporting Information. The atom numbering schemes used for the bond distances and bond orders are given in Figure 1. Charges and valencies are per atom in the designated rings. [b] The bond order is essentially zero. [c] Δ(m−n) denotes [total charge on atoms m−n of [1-M(CO)$_3$(η^4-E$_9$)]$^{4-}$] − [total charge on atoms m−n of E$_9^{4-}$].

actually predicted to be positive, with increased electron transfer to tungsten. The transition metal charges in the Sn clusters are negative: −0.95 for Cr, increasing to −1.27 for Mo, and then decreasing to −1.18 for W. The negative charges on the transition metals in the Pb$_9$ clusters are about half that of the Sn analogue and show an increase in the negative charge as the atomic number of the transition metal increases. There is a decrease of 0.11−0.13 (Sn, Pb) e on the apical E(1) atom, whereas the middle E(2,3,4,5) ring shows only a small change on the order of 0.03−0.05 (Sn) and 0.005−0.03 (Pb) e per atom. The valencies in the E$_9$ clusters show only small changes on complexation with the metal, suggesting a strong electrostatic interaction (Table 7). The valency for the Cr is about 7.0 (Sn) and 6.9 (Pb), as would be expected for interactions with four E atoms and three CO groups. The valencies for the Mo and W anions increase to 8.5−8.6 (Sn) and 7.9−8.3 (Pb).

There is less charge transferred from the Pb$_9$ cluster to the M(CO)$_3$ groups. The differences are most apparent for the Pb atom charges of the basal Pb(6,7,8,9) ring, which, unlike the Sn analogues, are always negative, and the charges on the transition metals, which are always less negative for [1-M(CO)$_3$(η^4-Pb$_9$)]$^{4-}$ than for [1-M(CO)$_3$(η^4-Sn$_9$)]$^{4-}$. This is also seen in the transition metal valencies and in the Pb−M bond orders, which are lower for the Pb$_9$ clusters.

Comparisons of the atomic charge differences between the E$_9^{4-}$ and [1-M(CO)$_3$(η^4-E$_9$)]$^{4-}$ anions, Δ(m−n) (Table 7), reveal that 86−93% of the charge that is delocalized onto the M(CO)$_3$ originates from the basal E(6,7,8,9) ring that is η^4-bonded to the transition metal. The apical E(1) atoms donate 6−9% of the delocalized charge, while the middle E(2,3,4,5) rings donate comparable amounts of charge, i.e., 1−10%. The large charge depletions from the E(6,7,8,9) rings are consistent with the assigned E−E spin−spin couplings and chemical shifts of the E$_4$ rings (see Characterization of the [1-M(CO)$_3$(η^4-Sn$_9$)]$^{4-}$ (M = Cr, Mo, W) and [1-Mo(CO)$_3$(η^4-Pb$_9$)]$^{4-}$ Anions by NMR Spectroscopy).

(c) NBO Populations. The NBO populations (Table 8) show that the valence s orbital populations do not change on complexation to M(CO)$_3$. The p orbital populations show a significant change, and it is from the p orbitals that the bulk of the charge is transferred to the M(CO)$_3$ fragment. For the E$_9$ fragment, the charge from the apical atom is transferred from the in-plane p orbital perpendicular to the C_4-axis of the E$_9$ cluster. There is very little change in the orbitals along the C_4-axis. The total p orbital populations in the middle ring change significantly for the [1-M(CO)$_3$(η^4-Sn$_9$)]$^{4-}$ series and show some charge transfer for the [1-M(CO)$_3$(η^4-Pb$_9$)]$^{4-}$ series. However, the charge-transfer per atom for the middle E(2,3,4,5) ring is smaller than the

Table 8. Natural Atomic Orbital Populations for the Valence Atomic Orbitals of the E_9^{4-} and $[1\text{-}M(CO)_3(\eta^4\text{-}E_9)]^{4-}$ (E = Sn, Pb; M = Cr, Mo, W) Anions

	Sn_9^{4-}			$Sn_9Cr(CO)_3^{4-}$				$Sn_9Mo(CO)_3^{4-}$				$Sn_9W(CO)_3^{4-}$			
	(1)	(2,3,4,5)	(6,7,8,9)	(1)	(2,3,4,5)	(6,7,8,9)	Cr	(1)	(2,3,4,5)	(6,7,8,9)	Mo	(1)	(2,3,4,5)	(6,7,8,9)	W
s	1.67	1.69	1.67	1.70	1.69	1.66	0.43	1.70	1.69	1.66	0.43	1.70	1.69	1.67	0.50
p_x	1.17	0.83	0.93	1.19	0.86	0.77		1.20	0.87	0.85		1.19	0.86	0.81	
p_y	0.86	0.88	1.09	0.74	1.01	0.77		0.75	0.73	0.87		0.74	0.98	0.98	
p_z	0.85	0.94	0.80	0.74	0.76	0.97		0.75	1.02	0.90		0.75	0.77	0.76	
d_{xy}							1.22				1.09				1.19
d_{xz}							1.21				1.09				1.18
d_{yz}							1.35				1.25				1.28
$d_{x^2-y^2}$							1.37				1.29				1.32
d_{z^2}							1.35				1.24				1.29
	Pb_9^{4-}			$Pb_9Cr(CO)_3^{4-}$				$Pb_9Mo(CO)_3^{4-}$				$Pb_9W(CO)_3^{4-}$			
	(1)	(2,3,4,5)	(6,7,8,9)	(1)	(2,3,4,5)	(6,7,8,9)	Cr	(1)	(2,3,4,5)	(6,7,8,9)	Mo	(1)	(2,3,4,5)	(6,7,8,9)	W
s	1.75	1.77	1.76	1.76	1.77	1.74	0.41	1.77	1.77	1.75	0.42	1.77	1.77	1.76	0.51
p_x	1.08	0.82	0.90	1.09	0.85	0.74		1.10	0.86	0.81		1.09	0.84	0.80	
p_y	0.86	0.85	1.04	0.77	0.85	0.66		0.76	0.77	0.72		0.77	0.81	1.01	
p_z	0.86	0.91	0.80	0.77	0.86	1.02		0.77	0.92	1.00		0.78	0.88	0.70	
d_{xy}							1.18				1.08				1.15
d_{xz}							1.18				1.09				1.16
d_{yz}							1.31				1.22				1.23
$d_{x^2-y^2}$							1.36				1.28				1.32
d_{z^2}							1.34				1.23				1.29

charge transfer for the apical E(1) atom. There is a significant charge transfer from the basal E(6,7,8,9) ring to the $M(CO)_3$ fragment. The largest amounts of charge transferred per basal E atom are for Cr (0.31 e for E = Sn and 0.32 e for E = Pb). The least amounts of charge transferred are for Mo, where the calculated amounts are 0.20 and 0.21 e for Sn and Pb, respectively. These values can be compared with transfers from the apical atom of 0.17−0.21 e for Sn and 0.16−0.17 e for Pb. The metal atoms have ∼0.4 e in the valence s orbitals of the lighter metals Cr and Mo and ∼0.5e in the s orbital of the W atom. The d orbital populations for all of the transition metals range from ∼1.1 to ∼1.4 e.

(d) Molecular Orbitals. The highest occupied molecular orbitals for Sn_9^{4-} are shown in Figure 7. The HOMO for the cluster is a degenerate orbital of E symmetry and is predominantly composed of radial p orbitals involving the Sn(6,7,8,9) atoms of the nido-face. The NHOMO[52] involves a set of radial p orbitals on the basal Sn(6,7,8,9) atoms that constructively interact to place a significant density in the center of the basal ring, perfectly suited for interacting with vacant orbitals on an incoming $M(CO)_3$ fragment. There is also some p character on the apical Sn(1) along the C_4-axis polarized toward the center of the cluster that is antibonding relative to the density in the center of the basal Sn(6,7,8,9) ring. The next orbital, HOMO-2, is degenerate with radial density in the basal and middle ring planes. The HOMO-3 orbital is essentially pure p in character along the C_4-axis with some small interactions with the basal Sn(6,7,8,9) atoms. The orbital HOMO-4 involves the bonding between the adjacent middle ring atoms, and there is a corresponding orbital, HOMO-6, for the basal ring atoms. Between is a doubly degenerate orbital, HOMO-5, involving the radial p orbitals on the apical Sn(1) atom that are perpendicular to the C_4-axis.

Several of the highest occupied molecular orbitals as well as the LUMO are depicted for $[1\text{-}Cr(CO)_3(\eta^4\text{-}Sn_9)]^{4-}$ in Figure 8. The focus of the discussion is on the orbitals involving the Sn_9 fragment and/or its interaction with the $Cr(CO)_3$ fragment that also provides a qualitative picture of the bonding of the $M(CO)_3$ and E_9 fragments for the remaining $[1\text{-}M(CO)_3(\eta^4\text{-}E_9)]^{4-}$ anions of the series considered in this study. The HOMO and NHOMO of $[1\text{-}Cr(CO)_3(\eta^4\text{-}Sn_9)]^{4-}$ are formed from the degenerate HOMO of the Sn_9 fragment, and there is a small delocalization of charge into the d_{xz} and d_{yz} orbitals of the transition metal. The next orbital, HOMO-2, involves a mixing of the d_{z^2} orbital on the Cr with the HOMO-3 orbital of the Sn_9 cluster so that the radial p orbital on the apical Sn(1) atom along the C_4-axis has some interaction with the transition metal atom. There are also some metal−carbonyl interactions in the HOMO-3. The HOMO-5 orbital involves the mixing of the NHOMO on the Sn_9 fragment with the d_{z^2} orbital on Cr, leading to a bonding interaction. The HOMO-6 orbital involves the interaction of the d_{xz} and d_{yz} orbitals with the HOMO-2 orbital of the Sn_9 cluster, again leading to a bonding interaction between the Sn_9 and $Cr(CO)_3$ fragments. The HOMO-12 orbital involves Cr−CO interactions as well as Cr−Sn interactions. The Sn_9^{4-} orbital involved in HOMO-12 of the transition metal cluster anion is HOMO-6. The final orbital that is shown is a very strongly polarized chromium d_{z^2} orbital interacting with the Sn_9 fragment. The LUMO of the anion involves an antibonding Cr−CO interaction coupled with a p orbital on the apical Sn(1) atom that is perpendicular to the C_4-axis. Several of the orbitals that are depicted place electron density within the cluster framework and possibly help account for the larger E−E nuclear spin−spin couplings observed between nonadjacent tin and lead atoms (see Characterization of the $[1\text{-}M(CO)_3$-

(52) NHOMO is defined as the next highest occupied molecular orbital, i.e., the second highest occupied molecular orbital. The remaining occupied orbitals are defined by their difference from the HOMO; for example, HOMO-2 is the third highest occupied molecular orbital.

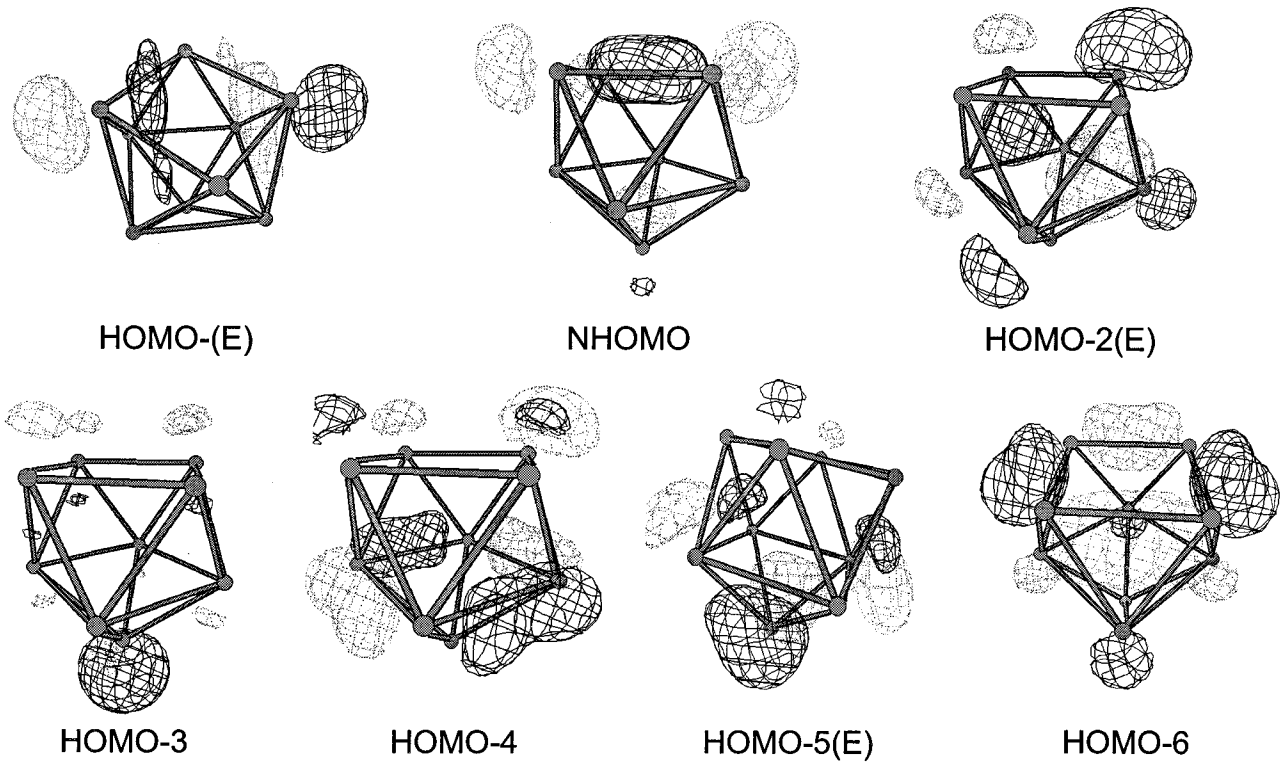

Figure 7. Wave function plots of the valence molecular orbitals for the Sn_9^{4-} anion at the LDFT level contoured at 0.04.

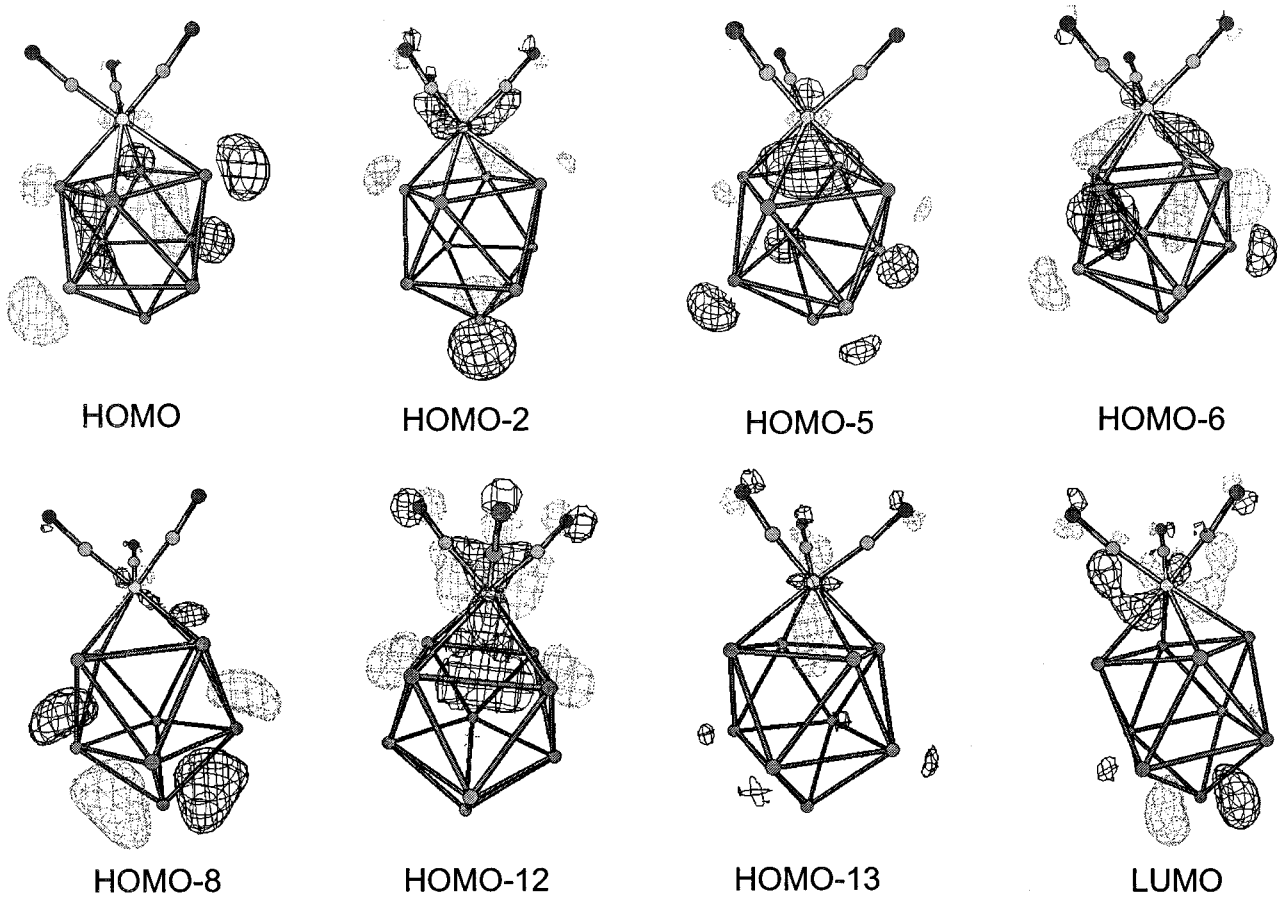

Figure 8. Wave function plots of the LUMO and valence molecular orbitals for the [1-Cr(CO)$_3$(η^4-Sn$_9$)]$^{4-}$ anion at the LDFT level contoured at 0.04.

(η^4-Sn$_9$)]$^{4-}$ (M = Cr, Mo, W) and [1-Mo(CO)$_3$(η^4-Pb$_9$)]$^{4-}$ Anions by NMR Spectroscopy).

(e) Infrared and Raman Spectra of the E_9^{4-} and [1-M(CO)$_3$(η^4-Sn$_9$)]$^{4-}$ Anions (E = Sn, Pb; M = Cr, Mo,

W). The experimental Raman and infrared frequencies and their assignments for the E_9^{4-} and [1-M(CO)$_3$(η^4-Sn$_9$)]$^{4-}$ anions are listed in Tables S3 and S4 of the Supporting Information, respectively, along with the calculated frequencies. The experimental Raman and infrared frequencies for [1-M(CO)$_3$(η^4-Sn$_9$)]$^{4-}$ are listed in the Experimental Section (Infrared Spectroscopy and Raman Spectroscopy).

(i) E_9^{4-}. The only experimental vibrational data reported thus far for the E_9^{4-} anions is for Sn_9^{4-} in K_4Sn_9 (99 and 146 cm^{-1}) and Cs_4Sn_9 (91, 102, 133, and 149 cm^{-1})[53] and for [2,2,2-crypt-K]$_4$[Sn$_9$] (108, 128, 148, 168 cm^{-1}; present work). Calculated vibrational frequencies have been previously reported for Pb_9^{4-}.[13]

The calculated vibrational frequencies for the Sn_9^{4-} and Pb_9^{4-} anions were derived from the fully optimized C_{4v} geometries of the anions at the LDFT level, and are all below 150 cm^{-1}, showing that the clusters are quite deformable. As expected, the Pb_9^{4-} modes appear at lower frequencies than those of Sn_9^{4-}. The experimental Raman spectrum of Sn_9^{4-} in the 2,2,2-crypt-K$^+$ salt comprises four broad peaks having frequencies that are in good agreement with the calculated values, although it is clear from their broadness that each of these peaks spans a range of frequencies. The calculated values are slightly underestimated. The low-frequency values indicate that there is little separability in terms of stretches, bends, torsions, etc., so we provide only general assignments.

(ii) [1-M(CO)$_3$(η^4-E$_9$)]$^{4-}$. The vibrational frequencies were calculated at the LDFT level for their fully optimized C_1 point group symmetries, which is also the symmetry observed for the [1-M(CO)$_3$(η^4-Sn$_9$)]$^{4-}$ anions in their crystal structures.

The three highest frequency modes are readily assigned to the CO stretches, with the highest frequency being assigned to the in-phase C−O stretch. The two low-frequency bands are approximately equal and are assigned to the out-of-phase C−O stretching modes, which are degenerate in an isolated M(CO)$_3$ fragment. There is good agreement between the calculated and observed values, with the calculated values being 30−80 cm^{-1} higher than the experimental values, as expected for calculated frequencies that do not include anharmonic corrections. As observed experimentally, the lowest C−O stretches are calculated for the Cr complexes, consistent with the largest d→π* interaction between the CO groups and the transition metal of lowest atomic number. With the exception of [1-Cr(CO)$_3$(η^4-Sn$_9$)]$^{4-}$, the three vibrational bands expected for the ν(C−O) modes are observed for each [1-M(CO)$_3$(η^4-E$_9$)]$^{4-}$ anion in the infrared spectra, which are in good agreement with the calculated values. As previously noted,[54,55] the observation of only two ν(C−O) bands for the precursors Cr(CO)$_3$·tol, Mo(CO)$_3$·mes, and W(CO)$_3$·mes[56] as well as for Mo(CO)$_3$(en)$_2$ and W(CO)$_3$(en)$_2$ (Table S4, footnotes *f* and *g*) can be attributed to the low effective masses of the organic groups coordinated to the M(CO)$_3$ moieties.

The carbonyl stretching frequencies in [1-M(CO)$_3$(η^4-E$_9$)]$^{4-}$ (1681−1830 cm^{-1}) (see Experimental Section, Infrared Spectroscopy) are shifted to lower frequencies relative to those of their M(CO)$_3$ precursors[56] and are among the lowest C−O stretching frequencies reported for terminally bonded metal carbonyls. The ν(CO) values of the [1-M(CO)$_3$(η^4-E$_9$)]$^{4-}$ anions are similar to those of the [1-M(CO)$_3$(η^4-Pn$_7$)]$^{3-}$ (Pn = P, As, Sb; M = Cr, Mo, W) anions.[55] The low ν(CO) values for [1-M(CO)$_3$(η^4-E$_9$)]$^{4-}$ are consistent with enhanced metal−CO d → π* back-bonding resulting from the buildup of negative charge on the transition metal atoms that results from electron donation from the E$_9$ cage into the frontier d orbitals of the metal (see (b) Charges and Valencies). The C−O stretches of the [1-M(CO)$_3$(η^4-Pb$_9$)]$^{4-}$ anions are lower in frequency than those of the corresponding [1-M(CO)$_3$(η^4-Sn$_9$)]$^{4-}$ anions, and this trend is reproduced in the calculated values. The experimental and calculated trends appear to be counterintuitive, however, suggesting that Pb_9^{4-} is a better π donor than Sn_9^{4-}. The trend is opposite to the conclusion drawn from a consideration of the changes in the calculated charge distributions in the E$_9$ cage and on the transition metal upon coordination of the M(CO)$_3$ group. The latter clearly shows that Sn_9^{4-} is the better π donor (see (b) Charges and Valencies). It appears that the relative CO stretching frequencies are not a reliable gauge of the relative π donor strengths of the coordinated E$_9$ cages.

The features in the range 417−698 cm^{-1} are mostly associated with M−C stretching motions and M−C−O bends. These modes were too weak to be observed in the Raman spectra of [1-M(CO)$_3$(η^4-Sn$_9$)]$^{4-}$. There are small contributions from the M−E stretches in several of these bands. The frequencies below 150 cm^{-1} are associated with the motions of the E$_9$ fragment: the E−M stretches; the C−M−C, E−M−C, and E−M−E bends; and the M(CO)$_3$ torsion. The torsional frequencies for rotation of the M(CO)$_3$ moieties relative to the basal planes of the E$_9$ cages are very low. This is in accord with the tin NMR spectra of the [1-M(CO)$_3$(η^4-Sn$_9$)]$^{4-}$ anions and the ^{207}Pb NMR spectrum of the [1-Mo(CO)$_3$(η^4-Pb$_9$)]$^{4-}$ anion, which are consistent with free rotation of the M(CO)$_3$ tripods (see Characterization of the [1-M(CO)$_3$(η^4-Sn$_9$)]$^{4-}$ (M = Cr, Mo, W) and [1-Mo(CO)$_3$(η^4-Pb$_9$)]$^{4-}$ Anions by NMR Spectroscopy). The ME$_9$ cage modes and various bends associated with the cage atoms are strongly coupled, preventing a simplified description of the modes, and further demonstrates that the M(CO)$_3$ and E_9^{4-} are rather strongly bonded. The experimental Raman spectra of the [1-M(CO)$_3$(η^4-Sn$_9$)]$^{4-}$ anions exhibit several broad lines in this region (see Experimental Section, Raman Spectroscopy) and, as in the case of the Sn_9^{4-} anion, each band is comprised of several overlapping bands. Again, the

(53) von Schnering, H. G.; Baitinger, M.; Carrillo-Cabrera, W.; Bolle, U.; Curda, J.; Grin, Y.; Heinemann, F.; Llanos, J.; Peters, K.; Schmeding, A.; Somer, M. *Z. Anorg. Allg. Chem.* **1997**, *623*, 1037.
(54) Deganello, G. In *Transition Metal Complexes of Cyclic Polyolefins;* Academic Press: New York, 1979; pp 197−199.
(55) Charles, S.; Eichhorn, B. W.; Rheingold, A. L.; Bott, S. *J. Am. Chem. Soc.* **1994**, *116*, 8077.

(56) The CO stretching frequencies for the transition metal carbonyl precursors are Cr(CO)$_3$·C$_6$H$_6$ (1970, 1894 cm^{-1}), Mo(CO)$_3$·mes (1957, 1883 cm^{-1}), and W(CO)$_3$·mes (1946, 1879 cm^{-1}).

experimental frequencies are in good agreement with the calculated ranges of values.

(f) Chemical Shifts. The standard used for the relative chemical shift calculations was $Sn(CH_3)_4$ (2934 ppm). Although the calculated chemical shifts are too high (Table 3), several experimental trends are correctly predicted. The apical Sn(1) is the most deshielded environment and is calculated to be deshielded by ~2000 ppm with respect to the Sn_4 planes, which is comparable with experiment. Most importantly, the weighted averages of the experimental and calculated (in parentheses) tin chemical shifts of Sn_9^{4-} and of the [1-M(CO)$_3$(η^4-Sn$_9$)]$^{4-}$ anion series exhibit the same trends, i.e., −1291.9 (−450) ppm, Sn_9^{4-} < −275.8 (715) ppm, W < −245.9 (777) ppm, Mo < −50 (895) ppm, Cr. As observed experimentally, the smallest Sn(1) chemical shift is that predicted for the Mo complex. The averages for the other eight Sn atoms are in error by 992, 1033, and 1080 ppm for Cr, Mo, and W, respectively, which are similar to the error in the average chemical shift for Sn_9^{4-}. The calculated differences in the chemical shifts of the two Sn_4 planes are small for the [1-M(CO)$_3$(η^4-Sn$_9$)]$^{4-}$ anion series (4−63 ppm) when compared with that calculated for Sn_9^{4-} (336 ppm) and therefore do not allow definitive assignments of the Sn_4 planes to be made for the [1-M(CO)$_3$(η^4-Sn$_9$)]$^{4-}$ anions whose experimental differences are much greater (239−308 ppm). It is noteworthy that only in the case of tungsten is the experimental trend reproduced. The differences between calculated and experimental values are attributed to the need for a better basis set and/or for the need to include relativistic effects. In addition, the calculated chemical shifts represent gas-phase values, and heavy atom chemical shifts display large solvent-induced effects on their chemical shifts that may be on the order of several hundred ppm (see Characterization of the [1-Mo(CO)$_3$(η^4-Pb$_9$)]$^{4-}$ Anion by NMR Spectroscopy and ref 50).

The fact that the apical chemical shift is significantly deshielded on complexation can be seen from many of the electronic structure indicators and is consistent with the "antipodal effect".[39,40] The large bond orders between the basal and apical atoms in the Sn_9 fragment suggest that significant changes in the electronic environment at the apical Sn(1) atom occur when charge is transferred from the basal Sn(6,7,8,9) ring to the metal on complexation. In addition, the significant bond order between the apical Sn(1) atom and M shows that the M further perturbs the electronic environment about the apical atom. In addition, the molecular orbitals of the Sn_9 fragment show a significant change on binding to the Cr(CO)$_3$ moiety. The NHOMO of the Sn_9^{4-} anion shows a radial p orbital along the C_4-axis mixing with a set of radial p orbitals in the basal plane, and most of the density on the apical atom is inside the Sn(6,7,8,9) ring (Figure 7). In contrast, this orbital in the complex (HOMO-5) has essentially no density on the apical atom (Figure 8). Rather, the HOMO-3 of Sn_9^{4-} is now the HOMO-2 of the Cr complex and mixes strongly with the d_{z^2} orbital on Cr. This orbital, which had more s character and was polarized essentially completely external to the ring, now has more p character and is only partially polarized external to the ring. As a consequence, there is a smaller contribution from the apical Sn(1) atom to the density inside the Sn(6,7,8,9) ring for the higher lying orbitals. These results all show a significant change in the electronic structure at the apical Sn(1) atom and are consistent with the large deshielding of the chemical shift that is observed upon coordination of the M(CO)$_3$ moiety.

(g) Coupling Constants. The magnitudes of $J(^{117,119}Sn-^{117,119}Sn)$ can be correlated with the s character in the skeletal bonding and are consistent with an enhanced Fermi contact contribution[57,58] to the tin−tin spin−spin couplings within these clusters. The Fermi contact contribution to the spin−spin coupling is proportional to the s electron densities at the coupled nuclei and is expected to be an important contributor to the spin−spin coupling mechanism when orbitals of high s character are involved in the coupling mechanism. The weighted averages for the $J(^{119}Sn-^{117}Sn)$ couplings of the nonfluxional [1-M(CO)$_3$(η^4-Sn$_9$)]$^{4-}$ anions, 589 Hz (Cr), 617 Hz (Mo), and 596 Hz (W), are significantly larger than the exchange averaged $J(^{119}Sn-^{117}Sn)$ coupling in Sn_9^{4-} (256 Hz, −10 °C in liquid NH_3 solvent) and in Sn_8Tl^{5-} (372 Hz, 30 °C in liquid NH_3 solvent). The NBO populations (vide supra) show that the s orbital populations remain unaltered upon coordination of the M(CO)$_3$ group to the Sn_9^{4-} and Pb_9^{4-} clusters with the donated electron density coming from the p orbitals. In the case of the [1-M(CO)$_3$-(η^4-Sn$_9$)]$^{4-}$ anions, the total p orbital populations are diminished over the triad by 1.53 (Cr), 1.10 (Mo), and 1.44 (W), with respect to those of Sn_9^{4-}, resulting in enhancement of the s character of the cluster bonding in these anions and corresponding increases in their average $J(^{119}Sn-^{117}Sn)$ couplings.

As noted above ((f) Chemical Shifts), there are significant bond orders between the basal and apical atoms in the Sn_9 moieties of the [1-M(CO)$_3$(η^4-Sn$_9$)]$^{4-}$ anions and between the apical atom and the transition metal. These interactions likely account for the fact that the $J(^{117,119}Sn-^{183}W)$ coupling between the two apical atoms, Sn(1) and W, is similar in magnitude to the coupling between W and the adjacent Sn-(6,7,8,9) plane. The observation that the $J(^{119}Sn-^{117}Sn)$ couplings between nonadjacent tin atoms are larger than between adjacent ones may be accounted for in similar terms.

Conclusion

The *closo*-[1-Mo(CO)$_3$(η^4-E$_9$)]$^{4-}$ and *closo*-[1-W(CO)$_3$(η^4-E$_9$)]$^{4-}$ cluster anions (E = Sn, Pb) have been structurally characterized in the solid state by vibrational spectroscopy and X-ray crystallography. The 22 ($2n + 4$) electron *nido*-E$_9^{4-}$ anions are found to η^4-coordinate the zero-electron donor groups M(CO)$_3$ (M = Cr, Mo, W) to their vacant apical positions, resulting in 10-atom ($2n + 2$) heteronuclear clusters that are based on bicapped square antiprisms. In contrast with the fluxional *nido*-Sn_9^{4-} and *nido*-Pb_9^{4-}, the MSn_9 cages of the *closo*-[1-M(CO)$_3$(η^4-Sn$_9$)]$^{4-}$ (M = Cr,

(57) Jameson, C. J. In *Multinuclear NMR*; Mason, J., Ed.; Plenum Press: New York, 1987; Chapter 4, p 89.
(58) Pople, J. A.; Santry, D. P. *Mol. Phys.* **1964**, *8*, 1.

Mo, W) anions have been shown by ^{119}Sn, ^{117}Sn, and ^{95}Mo NMR spectroscopy to be rigid and nonfluxional on the NMR time scale in liquid NH_3 solutions, whereas the $M(CO)_3$ groups are freely rotating. The simulation and summation of ^{119}Sn and ^{117}Sn subspectra arising from all possible isotopomer families and their absolute isotopomers have provided definitive assignments and interpretations of the complex satellite spectra that result from spin−spin coupling among the natural abundance ^{117}Sn, ^{119}Sn, and ^{183}W nuclides of the MSn_9. The ^{119}Sn and ^{117}Sn chemical shifts of the apical Sn atoms were significantly deshielded relative to those of both Sn_4 planes, and this finding is reproduced by GIAO calculations of the tin NMR shieldings. Lead-207 NMR studies of the [1-Mo(CO)$_3$(η^4-Pb$_9$)]$^{4-}$ anion in en and liquid NH_3 show that the fluxionality of the Pb_9 moiety has been modified. Density functional theory calculations at the local (LDFT) level have been used to derive the energy-minimized geometries of the E_9^{4-} and [1-M(CO)$_3$(η^4-E$_9$)]$^{4-}$ anions and to study the nature of the bonding in these anions, corroborate specific trends among their NMR chemical shifts, and assign the experimental infrared and Raman spectra of the Sn_9^{4-} and [1-M(CO)$_3$(η^4-Sn$_9$)]$^{4-}$ anions (M = Mo, W). The calculated charges and orbital populations show that the E_9 cages are π donors to the transition metal centers and that the E_4 plane bonded to the transition metal is the most charge-depleted, donating the bulk of the electron density to the transition metal.

Experimental Section

Apparatus and Materials. The majority of compounds used and prepared are highly air sensitive. Manipulations were performed under rigorously anhydrous conditions and in the absence of oxygen on a glass vacuum line or in a two-station nitrogen atmosphere drybox as previously described.[59]

Potassium metal (British Drug Houses, >99%) was cleaned as previously described,[60] and freshly cut samples were handled in a drybox. Lead shot (British Drug Houses, 99.9%), tin granules (Baker Analyzed Reagent, 99.9%), and 2,2,2-crypt (1,10-diaza-4,7,13,16,21,24-hexaoxabicyclo[8.8.8]hexacosane; Merck, 99%) were vacuum dried prior to handling in the drybox. Tricarbonylmesitylenemolybdenum(0) and tricarbonyltolylchromium(0) were prepared by heating $M(CO)_6$ [Alfa Inorganics, 99% (Mo), 98% (Cr)] in an excess of mesitylene (British Drug Houses, 99%) and toluene (British Drug Houses, 98%), respectively, under reflux in a nitrogen atmosphere, as described in refs 61 and 62. A small amount of dry tetrahydrofuran (THF) was added to wash any $M(CO)_6$ back into the reaction flask. The resulting precipitate was suction filtered and recrystallized from a CH_2Cl_2 (Caledon, 99.5%)/hexane (Caledon) mixture. Tricarbonylmesitylenetungsten(0) (Strem Chemicals, 98%) was transferred into the drybox as received and was exposed to the atmosphere of the drybox for at least 2 days prior to use.

All solvents were thoroughly dried, transferred by vacuum distillation, and stored in round-bottom flasks equipped with glass/Teflon stopcocks (J. Young). Ethylenediamine (Fisher Scientific, 99%) and tetrahydrofuran (Fisher, 99.9%) were initially dried over CaH_2 powder (British Drug Houses, 99.5%) and sodium pieces (British Drug Houses, 99.8%), respectively, for several weeks and then vacuum distilled onto and stored over fresh CaH_2 powder and sodium, respectively, for at least an additional week prior to use. Anhydrous ammonia (Matheson, 99.99%) was condensed under vacuum at −78 °C from the commercial cylinder into a previously vacuum-dried tube containing freshly cut sodium metal and stored at −78 °C for at least 1 week prior to use.

$KPb_{2.26}$ and $KSn_{2.05}$. The alloys were prepared as previously described:[12,13] $KPb_{2.26}$ (K, 0.4978 g, 12.73 mmol; Pb, 5.9621 g, 28.775 mmol), $KSn_{2.05}$ (K, 0.6356 g, 16.26 mmol; Sn, 3.9553 g, 33.325 mmol).

[1-M(CO)$_3$(η^4-E$_9$)]$^{4-}$ (E = Sn, Pb; M = Cr, Mo, W) Solutions for NMR Spectroscopy. Apparatus and techniques for NMR sample preparation have been previously described.[63] Solutions of the [1-M(CO)$_3$(η^4-Sn$_9$)]$^{4-}$ anions were prepared by reaction of deep red solutions of Sn_9^{4-}, which were obtained by extraction of the binary $KSn_{2.05}$ alloy in liquid NH_3, with a ca. 40% molar excess of Cr(CO)$_3$·tol or M(CO)$_3$·mes with respect to Sn_9^{4-}. The alloys were extracted for at least 1 week and the tricarbonyl complexes were added 1 day prior to sample isolation and NMR spectroscopic characterization. The following reagent amounts were used: [1-Cr(CO)$_3$(η^4-Sn$_9$)]$^{4-}$ ($KSn_{2.05}$, 0.1392 g, 0.4929 mmol; Cr(CO)$_3$·tol, 0.0456 g, 0.200 mmol), [1-Mo(CO)$_3$(η^4-Sn$_9$)]$^{4-}$ ($KSn_{2.05}$, 0.1556 g, 0.5510 mmol; Mo(CO)$_3$·mes, 0.0458 g, 0.153 mmol), [1-W(CO)$_3$(η^4-Sn$_9$)]$^{4-}$ ($KSn_{2.05}$, 0.1546 g, 0.5474 mmol; W(CO)$_3$·mes, 0.0701 g, 0.181 mmol). In the case of the [1-Mo(CO)$_3$(η^4-Pb$_9$)]$^{4-}$ solution, the $KPb_{2.26}$ alloy was extracted in both en ($KPb_{2.26}$, 0.1088 g, 0.214 mmol; Mo(CO)$_3$·mes, 0.0146 g, 0.049 mmol) and liquid NH_3 ($KPb_{2.26}$, 0.0972 g, 0.192 mmol; Mo(CO)$_3$·mes, 0.0164 g, 0.055 mmol).

Crystal Growth. Single crystals of [2,2,2-crypt-K]$^+$ salts of the [1-M(CO)$_3$(η^4-E$_9$)]$^{4-}$ anions that were suitable for X-ray structure determinations were grown from en solutions by slow vapor phase diffusion of THF into these solutions. Crystals were isolated and mounted as previously described;[64] specific details follow.

Solutions of Sn_9^{4-} were prepared by extraction of $KSn_{2.05}$ into en in the presence of 2,2,2-crypt. Addition of Mo(CO)$_3$·mes (0.0359 g, 0.119 mmol; ca. 40 mol % excess with respect to Sn_9^{4-}) to the red en extract containing 0.0948 g (0.252 mmol) of 2,2,2-crypt (ca 40 mol % deficit with respect to $KSn_{2.05}$; 0.1069 g, 0.3785 mmol) resulted in a red-brown solution. An analogous procedure was employed for the preparation of [1-W(CO)$_3$(η^4-Sn$_9$)]$^{4-}$ and [1-M(CO)$_3$(η^4-Pb$_9$)]$^{4-}$ (M = Mo, W) solutions for crystal growth. The following amounts of reagents were used: $KSn_{2.05}$ (0.1093 g, 0.3870 mmol), W(CO)$_3$·mes (0.0480 g, 0.124 mmol), and 2,2,2-crypt (0.0852 g, 0.226 mmol); $KPb_{2.26}$ (0.0935 g, 0.184 mmol), Mo(CO)$_3$·mes (0.0312 g, 0.104 mmol), and 2,2,2-crypt (0.1287 g, 0.3418 mmol); $KPb_{2.26}$ (0.0848 g, 0.167 mmol), W(CO)$_3$·mes (0.0407 g, 0.105 mmol), and 2,2,2-crypt (0.1222 g, 0.3246 mmol). The resulting solutions were also red-brown in color. After 24 h, THF was allowed to vapor diffuse into the en solutions over a period of several days. Large (>3 mm) parallelepiped crystals were isolated from the en/THF mixtures and were used for the crystal structure determinations. Note that the use of an excess or deficit (up to 20 mol %) of 2,2,2-crypt in the Mo and W tin solutions resulted in the immediate precipitation of amorphous material upon addition of liquid THF to the en solutions. Crystals used in this study had

(59) Borrmann, H.; Campbell, J.; Dixon, D. A.; Mercier, H. P. A.; Pirani, A. M.; Schrobilgen, G. J. *Inorg. Chem.* **1998**, *37*, 1929.
(60) Campbell, J.; DiCiommo, D. P.; Mercier, H. P. A.; Pirani, A. M.; Schrobilgen, G. J.; Willuhn, M. *Inorg. Chem.* **1995**, *34*, 6265.
(61) Muetterties, E. L.; Bleeke, J. R.; Sievert, A. C. *J. Organomet. Chem.* **1979**, *178*, 197.
(62) Nichols, B.; Whiting, M. C. *J. Chem. Soc.* **1959**, 551.
(63) Burns, R. C.; Devereux, L. A.; Granger, P.; Schrobilgen, G. J. *Inorg. Chem.* **1985**, *24*, 2615.
(64) Pirani, A. M.; Mercier, H. P. A.; Dixon, D. A.; Borrmann, H.; Schrobilgen, G. J. *Inorg. Chem.* **2001**, *40*, 4823.

the following dimensions: 0.51 × 0.44 × 0.33 mm^3 (Sn/Mo), 0.54 × 0.41 × 0.34 mm^3 (Sn/W), 0.57 × 0.39 × 0.25 mm^3 (Pb/Mo), and 0.52 × 0.43 × 0.31 mm^3 (Pb/W).

Multinuclear Magnetic Resonance Spectroscopy. The ^{119}Sn and ^{117}Sn (0 °C, NH_3) NMR spectra were recorded on a Bruker AC-300 (7.046 T) pulse spectrometer. The ^{95}Mo (0 °C, NH_3), ^{119}Sn (−70 °C, 0 °C, NH_3) and ^{207}Pb (0 °C, en and NH_3) NMR spectra were recorded on a Bruker AM-500 (11.744 T) pulse spectrometer. Spectra were routinely obtained without locking (field drift < 0.1 Hz h^{-1}) using 10-mm probes broad banded over the frequency ranges 14−121 MHz (7.046 T) and 23−202 MHz (11.744 T). The spectrometer frequencies were 32.593 MHz (^{95}Mo), 104.631 MHz (^{207}Pb), 106.945 MHz (^{117}Sn) and 111.922 MHz (^{119}Sn, 7.046 T). Free-induction decays were typically accumulated in 16K or 32K memories. Spectral width settings of 25 and 100 kHz were employed, yielding data point resolutions of 3.05 and 6.10 Hz/data point and acquisition times of 0.328 and 0.164 s, respectively. Relaxation delays were not applied. Typically, 10 000−100 000 transients were accumulated, depending on the concentrations and sensitivities of the nuclides under study. Pulse-width settings corresponding to a bulk magnetization tip angle, θ, of ∼90° were 12.5 (^{119}Sn), 13.0 (^{117}Sn), 25.0 (^{207}Pb), and 27.0 (^{95}Mo) μs. Line broadening parameters used in the exponential multiplication of the free induction decays were 3−10 Hz for the ^{117}Sn, ^{119}Sn, and ^{95}Mo NMR spectra and 50−100 Hz for the ^{207}Pb NMR spectra. Zero-filling to 128K of memory and 0−3 Hz line broadening factors were employed for resolution enhancement of the ^{119}Sn and ^{117}Sn Lorentzian lines and for observation of all *J* couplings. Variable-temperature spectra were recorded by using the variable-temperature controllers of the spectrometers, and temperatures (accurate to ± 1 °C and stable to within ± 0.1 °C) were checked by placing a copper constantan thermocouple into the sample region of the probes. Samples were allowed to equilibrate for at least 5 min while spinning before spectral accumulations were begun. The respective nuclei were referenced externally to samples of neat $(CH_3)_4$Pb, neat $(CH_3)_4$Sn, and 1 M aqueous Na_2MoO_4 at 30 °C. The chemical shift convention used was a positive (negative) shift signifies a chemical shift to high (low) frequency of the reference sample.

Simulation of NMR Spectra. The ^{117}Sn and ^{119}Sn NMR spectra of the [1-M(CO)$_3$(η^4-Sn$_9$)]$^{4-}$ (M = Cr, Mo, W) anions were simulated using the computer program ISOTOPOMER, as described previously.[44] The process begins with the calculation of the weight of each isotopomer family belonging to a cluster using binomial coefficients and the isotopic abundances. The program has a threshold option allowing the rejection of those isotopomer families whose percent abundances are less than or equal to a preselected value; the threshold applied for the simulations described in this work was 1 × 10^{-6} % relative abundance. The selected isotopomer families are further expanded into absolute isotopomers by taking all permutations of their isotopes among the sites within the molecule. The NMR Hamiltonian is then calculated for each of the absolute isotopomers and solved, and a subspectrum is calculated. The resultant subspectra are weighted according to their parent absolute isotopomer's weight and added together to produce the total simulated NMR spectrum for the cluster. Spectra in the present study were not iterated. The number of absolute isotopomers used for each environment is as follows: Sn(1), 4273 (Cr, Mo) and 4600 (W); Sn(2,3,4,5) or Sn(6,7,8,9), 10 989 (Cr, Mo) and 12 917 (W). The line widths were adjusted to fit the experimental spectrum. The chemical shifts and coupling constants used are those reported in Tables 3 and 4, respectively.

Infrared Spectroscopy. The FT infrared spectra were recorded on a Bio-Rad spectrometer (FTS-40) at ambient temperatures on KBr pellets. The KBr pellets were prepared in the drybox by mixing KBr, which had been previously dried under dynamic vacuum, with the M(CO)$_3$·mes precursors, crystals of the [2,2,2-crypt-K]$_4$[1-M(CO)$_3$(η^4-Sn$_9$)]·en, or M(CO)$_3$(en)$_2$ [2,2,2-crypt-K]$_4$[1-M(CO)$_3$-(η^4-Pb$_9$)]·2.5en (M = Mo, W). The resulting mixtures were pressed into pellets and sealed inside a chamber equipped with AgCl windows. The chamber was then placed inside the sample compartment of the spectrometer, which was closed and purged with dry N_2 gas for at least 15 min prior to data acquisition. The spectra consisted of 16 scans acquired with a resolution of ±4 cm^{-1} and a 5 kHz scan speed and were simultaneously subtracted from the background which was recorded prior to spectral acquisition: Sn/Mo, 1703, 1718, 1830 cm^{-1}; Sn/W, 1701, 1711, 1822 cm^{-1}; Pb/Mo, 1702, 1736, 1813 cm^{-1}; Pb/W, 1686, 1697, 1804 cm^{-1}.

Raman Spectroscopy. The FT Raman spectra of the [1-M(CO)$_3$-(η^4-Sn$_9$)]$^{4-}$ (M = Mo, W) salts were recorded on a Bruker Equinox 55/FRA 106 spectrometer as described previously.[65] The spectra were recorded at −100 °C using a defocused laser spot of 400 mW (15% less at the sample) power. Eight (Mo) and four (W) blocks of 500 scans were averaged for a combined acquisition time of 120 (Mo) and 60(W) min. The randomly orientated single crystals were sealed in Pyrex Lindeman capillaries inside a drybox; the capillaries had been previously dried at 250 °C under vacuum for at least 1 day. The Raman spectrum of the Sn_9^{4-} anion salt was recorded on a Bruker RFS 100 FT Raman spectrometer as described previously.[66] The spectrum was recorded at −130 °C using a laser power of 178 mW and averaged over 400 scans. The sample was a microcrystalline powder sealed in a Pyrex melting point capillary inside a drybox; the capillary had been previously dried at 250 °C under vacuum for at least 1 day. The spectral resolutions were 4 cm^{-1}: Sn/Mo, 93, 100, 108, 117, 124, 140 cm^{-1}; Sn/W, 83, 92, 108, 124, 139, 164 cm^{-1}.

X-ray Crystallography. (a) Collection and Reduction of X-ray Data. The data sets were collected on a P4 Siemens diffractometer equipped with a Siemens SMART 1K CCD area detector and a rotating anode with graphite-monochromated Mo Kα radiation (λ = 0.71073 Å) using the program SMART.[67] The diffraction data collection consisted of a full ψ rotation at χ = 0° using (1200 + 50) 0.3° frames, followed by a series of short (100 frames) ϖ scans at various χ and ψ settings to fill the gaps. The detector was located at 3.991 cm from the crystal, and a complete data set was acquired at a 2θ setting of 330°. A complete sphere of data was collected, to better than 0.8 Å resolution. The data were reduced with the program SAINT,[67] which applied Lorentz and polarization corrections to the three-dimensionally integrated diffraction spots. The program SADABS[68] was used for the scaling of the diffraction data and the application of an empirical absorption correction based on redundant reflections.

(b) Solution and Refinement of the Structures. The Siemens SHELXTL PLUS[69] software package was used for the solution and refinement of the crystal structures. The XPREP[69] program was used to confirm the unit cells and the crystal lattices. Direct methods were used to solve the structures in the appropriate space groups which generally located the positions of the polyanions and most

(65) Borrmann, H.; Campbell, J.; Dixon, D. A.; Mercier, H. P. A.; Pirani, A. M.; Schrobilgen, G. J. *Inorg. Chem.* **1998**, *37*, 6656.
(66) Fir, B. A.; Mercier, H. P. A.; Sanders, J. C. P.; Dixon, D. A.; Schrobilgen, G. J. *J. Fluorine Chem.* **2001**, *110*, 89.
(67) SMART and SAINT, Release 4.05, Siemens Energy and Automation Inc., Madison, WI, 1994.
(68) Sheldrick, G. M., Siemens Area Detector Absorption Corrections (SADABS), Personal communication, 1996.
(69) Sheldrick, G. M., SHELXTL-Plus, Release 5.03, Siemens Analytical X-ray Instruments Inc., Madison, WI, 1994.

of the non-hydrogen atoms of the (2,2,2-crypt-K^+) cations. Full-matrix least-squares refinements of the positions and isotropic thermal parameters of the assigned atoms and successive difference Fourier syntheses revealed the positions of the remaining non-hydrogen atoms of (2,2,2-crypt-K^+) and any solvent molecules. In the crystal structure of [2,2,2-crypt-K]$_4$[1-Mo(CO)$_3$(η^4-Sn$_9$)]·en, two (2,2,2-crypt-K^+) cations were found to be disordered. The disorder was treated by using a rigid body refinement (FRAG in the program SHELXTL PLUS[69]). Disordered solvent molecules were generally not located until the atoms of the anions and/or cations were refined with anisotropic thermal parameters. The final structure solutions involved the refinement of the non-hydrogen atoms of nondisordered anions, cations, and solvent molecules with anisotropic thermal parameters (Supporting Information), assigning the calculated positions of the hydrogen atoms [d(C−H) = 0.96 Å, U_{iso}(H) fixed to 1.2U_{eq}(C)], and by setting the weight factor to the recommended values.

Computational Results. The calculations were done at the density functional theory (DFT) level.[70−74] The DFT geometry optimizations and frequency calculations were done with the program Dgauss[75−77] on SGI computers. The calculations were done at the local level with the potential fit of Vosko et al.[78] for correlation and Slater exchange.[79] The calculations were done with the following basis sets: for Sn, a double-ζ basis set was used with the ECP of Kuechle et al.;[80] for Pb, a polarized double-ζ basis set was used with the ECP of Kuechle et al.;[80] for Cr, C, and O, the DZVP2 polarized double-ζ basis set was used;[81] and for Mo and W, the 6s5p3d basis set with the ECP of Kuechle was used.[80] The A1 fitting set or the fitting sets derived for pseudopotentials within DGauss were used.[82,83] The geometries were optimized by using analytic gradient methods, and second derivatives were also calculated analytically. Atomic valencies following Mayer[84−87] were calculated. In addition, natural bond orbital (NBO) analyses[88−92] were done with the program Gaussian 98.[93] These calculations were done at the local level with the basis sets given above with the following changes: for Sn, a set of d polarization functions was added,[94] and the DZVP basis set was used for C, O, Cr, and Mo. The NMR calculations for Sn were done with the program Gaussian 98[93] using the GIAO approach for treating the origin problem.[95−98] The calculations were done with the DZVP basis set of Godbout et al.,[81] except for W, where the effective core potential (ECP) of the Stuttgart group with their basis set[99] was used. Sixty electrons were included in the W ECP, the so-called small core ECP.

Acknowledgment. We thank the Natural Sciences and Engineering Research Council (NSERC) of Canada for support in the form of a research grant. We also thank NSERC and the Ontario Ministry of Education and Training for the award of graduate scholarships to J.C. and the German Academic Exchange Service (DAAD) for the award of a travel grant to H.F. We acknowledge Dr. Charles F. Campana of Bruker AXS, Inc., Madison, WI, for acquiring a data set for (CO)$_3$Mo(en)$_2$[2,2,2-crypt-K]$_4$[1-Mo(CO)$_3$(η^4-Pb$_9$)]·2.5en and Nancy Kawai of Bruker Optics, Billerica, MA, for recording the Raman spectra of the [1-M(CO)$_3$(η^4-Sn$_9$)]$^{4-}$ (M = Mo, W) salts. The density functional theory calculations were performed, in part, in the Molecular Sciences Computing Facility (MSCF), William R. Wiley Environmental Molecular Sciences Laboratory, Pacific Northwest National Laboratory. The MSCF is funded by the Office of Biological and Environmental Research, U.S. Department of Energy. The Pacific Northwest National Laboratory is operated by Battelle for the U.S. Department of Energy under Contract DE-AC06-76RLO 1830.

Supporting Information Available: The [2,2,2-crypt-K^+-en] cation in [2,2,2-crypt-K]$_4$[1-M(CO)$_3$(η^4-Sn$_9$)]·en (Figure S1); the Mo(CO)$_3$(en)$_2$ complex in (CO)$_3$Mo(en)$_2$[2,2,2-crypt-K]$_4$[1-M(CO)$_3$-(η^4-Pb$_9$)]·2.5en (Figure S2); the ^{207}Pb (104.613 MHz) NMR spectra of the Sn(1), Sn(2,3,4,5), and Sn(6,7,8,9) environments in the [1-Mo(CO)$_3$(η^4-Pb$_9$)]$^{4-}$ anion (Figure S3); complete set of nonaveraged calculated bond lengths and bond angles (Table S1) and Mayer valencies, Mayer bond orders, and Mulliken Charges (Table S2) for the E$_9^{4-}$ and [1-M(CO)$_3$(η^4-E$_9$)]$^{4-}$ anions (E = Sn, Pb; M = Cr, Mo, W]; experimental and calculated frequencies and

(70) Parr, R. G.; Yang, W. *Density Functional Theory of Atoms and Molecules*; Oxford University Press: New York, 1989.
(71) Labanowski, J.; Andzelm, J., Eds. *Density Functional Methods in Chemistry*; Springer-Verlag: New York, 1991.
(72) Ziegler, T. *Chem. Rev.* **1991**, *91*, 651.
(73) Salahub, D. R. In *Ab Initio Methods in Quantum Chemistry−II*; K. P. Lawley, Ed.; J. Wiley & Sons: New York, 1987; p 447.
(74) Jones, R. O.; Gunnarsson, O. *Rev. Mod. Phys.* **1989**, *61*, 689.
(75) Andzelm, J. W.; Wimmer, E.; Salahub, D. R. In *The Challenge of d and f Electrons: Theory and Computation*; Salahub, D. R., Zerner, M. C., Eds.; ACS Symposium Series 394, American Chemical Society: Washington DC, 1989; p 228.
(76) Andzelm, J. In *Density Functional Theory in Chemistry*; Labanowski, J. K., Andzelm, J. W., Eds.; Springer-Verlag: New York, 1991; pp 155−174.
(77) Andzelm, J. W.; Wimmer, E. *J. Chem. Phys.* **1992**, *96*, 1280. DGauss is a density functional program which is part of Unichem and is available from Oxford Molecular.
(78) Vosko, S. H.; Wilk, L.; Nusair, M. *Can. J. Phys.* **1980**, *58*, 1200.
(79) Slater, J. C. *Phys. Rev.* **1951**, *81*, 385.
(80) Kuechle, W.; Dolg, M.; Stoll, H.; Preuss, H. *Mol. Phys.* **1991**, *74*, 1245.
(81) Godbout, N.; Salahub, D. R.; Andzelm, J. W.; Wimmer, E. *Can. J. Chem.* **1992**, *70*, 560.
(82) Chen, H.; M. Krasowski, M.; Fitzgerald, G. *J. Chem. Phys.* **1993**, *98*, 8710.
(83) Lee, C.; Chen, H. Unpublished results. See the UniChem manual, Versions 3.0−5.0.
(84) Mayer, I. *Chem. Phys. Lett.* **1983**, *97*, 270.
(85) Mayer, I. *Theor. Chim. Acta* **1985**, *67*, 315.
(86) Mayer, I. *Int. J. Quantum Chem.* **1986**, *29*, 73.
(87) Mayer, I. *Int. J. Quantum Chem.* **1986**, *29*, 477.
(88) Reed, A. E.; Curtiss, L. A.; Weinhold, F.*Chem. Rev.* **1988**, *88*, 899.
(89) Foster, J. P.; Weinhold, F. *J. Am. Chem. Soc.* **1980**, *102*, 7211.
(90) Reed, A. E.; F. Weinhold, F. *J. Chem. Phys.* **1983**, *78*, 4066.
(91) Reed, A. E.; Weinstock, R. B.; Weinhold, F. *J. Chem. Phys.* **1985**, *83*, 735.
(92) Reed, A. E.; Weinhold, F. *J. Chem. Phys.* **1985**, *83*, 1736.
(93) Frisch, M. J.; Trucks, G. W.; Schlegel, H. B.; Scuseria, G. E.; Robb, M. A.; Cheeseman, J. R.; Zakrzewski, V. G.; Montgomery, J. A.; Stratmann, R. E.; Burant, J. C.; Dapprich, S.; Millam, J. M.; Daniels, A. D.; Kudin, K. N.; Strain, M. C.; Farkas, O.; Tomasi, J.; Barone, V.; Cossi, M.; Cammi, R.; Mennucci, B.; Pomelli, C.; Adamo, C.; Clifford, S.; Ochterski, J.; Petersson, G. A.; Ayala, P. Y.; Cui, Q.; Morokuma, K.; Malick, D. K.; Rabuck, A. D.; Raghavachari, K.; Foresman, J. B.; Cioslowski, J.; Ortiz, J. V.; Stefanov, B. B.; Liu, G.; Liashenko, A.; Piskorz, P.; Komaromi, I.; Gomperts, R.; Martin, R. L.; Fox, D. J.; Keith, T.; Al-Laham, M. A.; Peng, C. Y.; Nanayakkara, A.; Gonzalez, C.; Challacombe, M.; Gill, P. M. W.; Johnson, B.; Chen, W.; Wong, M. W.; Andres, J. L.; Gonzalez, A. C.; Head-Gordon, M.; Replogle, E. S.; Pople, J. A. *Gaussian 98*, A.6; Gaussian, Inc.: Pittsburgh, PA, 1998.
(94) Huzinaga, S.; Andzelm, J.; Klobukowski, M.; Radzio-Andzelm, E.; Sakai, Y.; tatewaki, H. *Gaussian Basis Sets for Molecular Calculations*; Physical Sciences Data Series 16; Elsevier: Amsterdam, 1984.
(95) Cheeseman, J. R.; Trucks, G. W.; Keith, T. A.; Frisch, M. J. *J. Chem. Phys.* **1996**, *104*, 5497.
(96) London, F. *J. Phys. Radium* (Paris) **1937**, *8*, 397.
(97) Ditchfield, R. *Mol. Phys.* **1974**, *27*, 789.
(98) Wolinski, K.; Hinton, J. F.; Pulay, P. *J. Am. Chem. Soc.* **1990**, *112*, 8251.
(99) Kuechle, W.; Dolg, M.; Stoll, H.; Preuss, H. *J. Chem. Phys.* **1994**, *100*, 7535 and references therein.

assignments for the E_9^{4-} (Table S3) and [1-M(CO)$_3$(η^4-E$_9$)]$^{4-}$ (Table S4) anions (E = Sn, Pb; M = Cr, Mo, W]; and an X-ray crystallographic file in CIF format for the structure determinations of (CO)$_3$M(en)$_2$[2,2,2-crypt-K]$_4$[1-M(CO)$_3$(η^4-Pb$_9$)]·2.5en and [2,2,2-crypt-K]$_4$[1-M(CO)$_3$(η^4-Sn$_9$)]·en, where M = Mo, W. This material is available free of charge via the Internet at http://pubs.acs.org.

IC010695K